Supplementary material for:

The structural basis for an on-off switch controlling Gβγ-mediated inhibition of TRPM3 channels

Marc Behrendt[a,b,1,2], Fabian Gruss[c,1,3], Raissa Enzeroth[a,b], Sandeep Dembla[a,b], Siyuan Zhao[d], Pierre-Antoine Crassous[d], Florian Mohr[a], Mieke Nys[c], Nikolaos Louros[e], Rodrigo Gallardo[e,4], Valentina Zorzini[f,5], Doris Wagner[a], Anastassios Economou[f], Frederic Rousseau[e], Joost Schymkowitz[e], Stephan E. Philipp[g], Tibor Rohacs[d], Chris Ulens[c,6], Johannes Oberwinkler[a,b,6]

[a] Institut für Physiologie und Pathophysiologie, Philipps-Universität Marburg, 35037 Marburg, Germany
[b] Center for Mind, Brain and Behavior (CMBB), Philipps-Universität Marburg and Justus-Liebig-Universität Giessen, 35032 Marburg, Germany
[c] Laboratory of Structural Neurobiology, Department of Cellular and Molecular Medicine, KU Leuven, 3000 Leuven, Belgium
[d] Department of Pharmacology, Physiology and Neuroscience, Rutgers New Jersey Medical School, Newark, NJ 07103
[e] Switch Laboratory, VIB Center for Brain and Disease Research, Department of Cellular and Molecular Medicine, KU Leuven, 3000 Leuven, Belgium
[f] Laboratory of Molecular Bacteriology, Department of Microbiology and Immunology, Rega Institute for Medical Research, KU Leuven, 3000 Leuven, Belgium
[g] Experimentelle und Klinische Pharmakologie und Toxikologie, Universität des Saarlandes, 66421 Homburg, Germany

[1] M.B. and F.G. contributed equally to this work.
[2] Present address: Experimental Pain Research, Heidelberg University, Medical Faculty Mannheim, 68167 Mannheim, Germany
[3] Present address: Hubrecht Institute, Royal Netherlands Academy of Arts and Sciences, 3854 CT Utrecht, The Netherlands
[4] Present address: Astbury Centre for Structural Molecular Biology, School of Molecular and Cellular Biology, University of Leeds, Leeds LS2 9JT, United Kingdom
[5] Present address: Sir William Dunn School of Pathology, University of Oxford, Oxford OX1 3RE, United Kingdom

[6] To whom correspondence may be addressed.
Email: chris.ulens@kuleuven.be or johannes.oberwinkler@uni-marburg.de

Contents:

www.pnas.org/cgi/doi/10.1073/pnas.2001177117

Supplementary Materials and Methods

Expression and purification of $G\beta_1\gamma_2$(C68S): Mouse $G\beta_1$ wild-type cDNA was cloned untagged into a pFastBac vector with a SLIC cloning approach for expression in Sf9 insect cells via the Bac-to-Bac system (Invitrogen, Carlsbad, California, USA). Mouse $G\gamma_2$ was also cloned into a pFastBac vector, carrying a sequence encoding for an N-terminal 8xHis-tag followed by a thrombin cleavage site. A single point mutation was introduced using the QuikChange protocol (Agilent, Santa Clara, California, USA), resulting in a $G\gamma_2$(C68S) variant (1). This mutation prevents the attachment of a geranylgeranyl lipid modification and thus renders the Gβγ protein complex water soluble. Throughout the main text of this manuscript, we refer to the $G\beta_1\gamma_2$(C68S) protein complexes as "water-soluble Gβγ". The correctness of the cloned constructs was confirmed by DNA sequencing. The applied construct design and expression strategies were inspired by the protocols described in refs 1 and 2. For both constructs viruses were amplified and P3 viruses were produced in Sf9 cells using established protocols. For $G\beta_1\gamma_2$(C68S) expression Sf9 cells were coinfected with $G\beta_1$ and $G\gamma_2$(C68S) P3 viruses. A good ratio between the viruses was determined with initial purifications (as described below) from medium scale expressions using different ratios of the viruses to infect the cells.

For Gβγ(C68S) large scale preparations 3 to 6 l of around 10^6 / ml Sf9 cells in Insect-Xpress medium (Lonza, Basel, Switzerland) were coinfected with 200 µl $G\beta_1$ P3 virus and 100 µl $G\gamma_2$(C68S) P3 virus per 100 ml cells. After 3 days orbital shaking of the suspension culture at 28 °C, the cell pellet was collected by centrifugation at 10,000 x g for 20 min. and either used directly or flash frozen in liquid nitrogen and stored at −80 °C. The cell pellet expressing Gβγ(C68S) was resuspended in about twice the volume Tris buffer (50 mM Tris-HCl, pH 7.5 at 4 °C, 200 mM NaCl) containing 1 mM PMSF, 1 µg / ml aprotinin, 1 µg / ml pepstatin, 1 µg / ml leupeptin, 5 mM $MgCl_2$, 20 µg / ml DNase I and 5 mM Tris(2- carboxyethyl)phosphin (TCEP), and lysed by two rounds in the EmulsiFlex-C5 homogenizer (Avestin, Mannheim, Germany). After centrifugation for 1 h at 180,000 x g at 4 °C, 20 mM imidazole was added to the supernatant, which was then incubated with 4 ml Ni^{2+} Sepharose 6 Fast Flow beads (GE Healthcare, Chicago, Illinois, USA) rotating for 1 h at 4 °C. The beads were centrifuged for 20 min. at 500 x g at 4 °C and the supernatant discarded. The beads were resuspended in Tris buffer containing 20 mM imidazole and 5 mM TCEP, transferred to a column and then washed with 3 x 20 ml of the same buffer. 8 ml of the buffer and 100 units of thrombin (Merck, Darmstadt, Germany) were added to the beads for incubation overnight, rotating at 4 °C. The flow-through from the beads containing the cleaved protein [N-terminal 8xHis-tag removed from $G\gamma_2$(C68S)] was then collected and pooled with an additional 8 ml wash of the beads with the same buffer. This sample was slightly

cloudy and therefore centrifuged for 20 min. at 20,000 x g at 4 °C. The clear supernatant was concentrated with Amicon Ultra–15 10K centrifugal concentrators (Merck). About 1/20 of a SigmaFast EDTA-free inhibitor cocktail tablet (Merck) was added to the sample to inhibit remaining thrombin. Final sample polishing was done on a Superdex 200 Increase 10/300 GL size exclusion column (GE Healthcare) in 20 mM Tris-HCl pH 7.5 (at 4 °C), 150 mM NaCl, 5 mM DTT (for cocrystallization experiments) or 5 mM TCEP (for bio-layer interferometry and Ni^{2+} column pull-down experiments). Peak fractions were analyzed by SDS-PAGE, selected for purity, pooled and concentrated to the desired protein concentration with a typical final yield of 1 to 2 mg Gβγ(C68S) per 1 l cell culture. This final sample was either used directly or flash frozen in liquid nitrogen and stored at −80 °C.

Expression and purification of TRPM3 exon 17-encoded peptide fused to His-tagged maltose-binding protein

Maltose-binding protein with an N-terminal 6xHis-tag was cloned into a plasmid for bacterial expression containing an IPTG-inducible promotor. C-terminal to the maltose-binding protein, DNA encoding for a thrombin binding site (GLVPRGS) followed directly by DNA encoding for TRPM3 exon17 peptide with 2 N-terminal and 3 C-terminal flanking residues (K_{592}RPKALKLLGMEDDI$_{606}$; exon 17-encoded residues underlined) was cloned in. The correctness of the cloned construct was confirmed by DNA sequencing. Chemically competent *E. coli* BL21(DE3) were transformed with this plasmid according to standard procedures. A pre-culture of LB media containing the selection marker antibiotic carbenicillin was grown over night at 37 °C with orbital shaking. The next day, 4 l LB with carbenicillin were inoculated with pre-culture to an OD_{600} of 0.2 and incubated at 37 °C with orbital shaking. When the OD_{600} reached a value of 0.6 to 0.8, 0.8 mM IPTG was added to induce the expression of the maltose-binding protein construct, and the cells were harvested 4 hours later by centrifugation at 10,000 x g for 10 min. The cell pellet was either used directly or frozen in liquid nitrogen and stored at −80 °C. The cell pellet was resuspended in about twice the volume Tris buffer (50 mM Tris-HCl, pH 7.5 at 4 °C, 200 mM NaCl) containing 1 mM PMSF, 1 µg / ml aprotinin, 1 µg / ml pepstatin, 1 µg / ml leupeptin, 5 mM $MgCl_2$, 20 µg / ml DNase I and 1 mg/ml lysozyme, and lysed by two rounds in the EmulsiFlex-C5 homogenizer (Avestin). After centrifugation for 30 min. at 27,000 x g at 4 °C, 20 mM imidazole was added to the supernatant, which was then incubated with 4 ml Ni^{2+} Sepharose 6 Fast Flow beads (GE Healthcare) rotating for 45 min. at 4 °C. The flow-through from the beads was discarded and the beads were then washed with 3x 20 ml of Tris buffer containing 20 mM imidazole, 1 mM PMSF, 1 µg / ml aprotinin, 1 µg / ml pepstatin, and 1 µg / ml leupeptin. The protein was eluted from the beads with 2x 7.5 ml of the same buffer with 300 mM imidazole. The sample was then incubated with 3 ml amylose re-

sin (New England BioLabs, Ipswich, Massachusetts, USA) rotating for 45 min. at 4 °C. The flow-through from the beads was discarded and the beads were then washed with 2x 20 ml of Tris buffer. The protein was eluted from the beads with 2x 7.5 ml of Tris buffer with 50 mM maltose. The eluate was concentrated with Amicon Ultra–15 10K centrifugal concentrators (Merck). Final sample polishing was done on a Superdex 75 10/300 GL size exclusion column (GE Healthcare) in 20 mM Tris-HCl, pH 7.5 (at 4 °C), 150 mM NaCl. Peak fractions were analyzed by SDS-PAGE, selected for purity, pooled and concentrated to the desired protein concentration with a typical final yield of 2.5 mg maltose-binding protein construct per 1 l bacterial culture. This final sample was either used directly or flash frozen in liquid nitrogen and stored at −80 °C.

Dot blot analysis

Dot blot analysis was performed similar as described (3) with 25-mer polypeptides synthesized on polyethlylenglycol-derivatized cellulose membranes (amino-PEG500-UC540, Intavis AG, Cologne, Germany) using an Intavis ResPepSL peptide spot synthesizer using the amount of 40 µg peptide per spot (diameter: 3 mm). The blots were washed three times in 100 ml BPTL buffer containing 50 mM Tris-HCl, 150 mM NaCl, 10 mM EDTA, 0.1 % Triton X-100 (pH 7.5) for 10 min. at room temperature and incubated overnight in BPTL buffer containing 60 µg purified His-tagged Gβγ proteins / ml at 4 °C while gently rocking. Blots were washed three times, blocked for 1 h in 5 % milk powder / BPTL and incubated with anti-Gβ antibodies (1:500, sc-378, Santa Cruz, Heidelberg, Germany) for 2 h at room temperature. Blots were washed again three times with BPTL buffer and incubated for 1 h at room temperature with a secondary horseradish peroxidase-conjugated goat-anti-rabbit antibody. After three washes with BPTL, signals were detected using the Western Lightning Chemiluminescence Reagent Plus Kit (Perkin Elmer, Waltham, Massachusetts, USA) and a cooled CCD system (LAS-3000, Fujifilm, Düsseldorf, Germany). Nonsaturated signals were quantified densitometrically using the AIDA 3.0 software (Elysia-Raytest, Straubenhardt, Germany).

Construction of cDNA clones

We generated, using PCR-based standard methods and oligonucleotides from Eurofins (Ebersberg, Germany), a number of TRPM3-based constructs with various tags in several different mammalian expression vectors. Specifically: N-terminally YFP-tagged mouse TRPM3α5 (YFP-TRPM3α5) was created by deletion of 30 base pairs (corresponding to exon 17) from mouse YFP-TRPM3α2 in pcDNA3 (4), as the 30 base pairs encoded by exon 17 are the sole difference between these two splice variants. We generated N-terminally triple FLAG-tagged versions of mouse splice variants by using previously published clones of the different

TRPM3-YFP splice variants (4, 5) and subcloning into pCMV-3Tag-1 (Agilent, Santa Clara, California, USA).

Truncated TRPM3α2 and TRPM3α5 constructs (*SI Appendix*, Fig. S1) were also generated from previously published clones (5, 6) by PCR amplification, mutagenesis PCR and subcloning in pCMV-3Tag-3 vectors (Agilent). These constructs are missing exon 1 and 3 from TRPM3α2 or TRPM3α5 (which do in themselves not contain sequences from exon 2, see Fig. 1*D*). Therefore, the protein sequences of these constructs start with an additional methionine and the first amino acids of exon 4 (C_{89}, yielding an N-terminal sequence of MC_{89}CCGRL). These truncated TRPM3α2 and TRPM3α5 constructs are also shortened at the C-terminus and end with the beginning of exon 28 (ending with $PTSP_{1330}$) followed by a triple FLAG-tag sequence.

The cDNA for human μOR (in pcDNA3.1) was purchased from the cDNA Resource Center (Bloomsburg, PA, USA) and subcloned in pCAGGS-IRES-GFP, the IRES-GFP cassette enabling easy identification of transfected cells. We generated the fusion construct Myc-$G\beta_1$ (in pcDNA3.1) starting from human $G\beta_1$ cDNA (4, 7). Mutants of murine TRPM3α2 and human $G\beta_1$ were generated by mutagenesis PCR (oligonucleotide primers from Eurofins) utilizing the plasmids TRPM3α2-YFP in pcDNA3 (4) and the previously generated Myc-$G\beta_1$, respectively. $G\beta_1$ mutants for expression in *Xenopus laevis* oocytes were generated using the Quik-Change mutagenesis kit (Agilent, Santa Clara, California, USA). Direct sequencing was performed by Seqlab (Göttingen, Germany) to verify the correctness of manipulated DNA sequences.

Generation of a HEK293 cell line stably expressing murine YFP-TRPM3α5

The generation of this cell line was performed essentially as published (8). HEK293 cells were transfected using Metafectene Pro obtained from Biontex (Martinsried, Germany) following the manufacturer's instructions and split the following day. Selection of cells stably expressing the construct was performed in the presence of 0.5 mg / ml geneticin (Sigma-Aldrich, Munich, Germany), which was added the day after splitting. After 14 – 21 days, colonies were isolated, subcultured and stable transformants were screened by YFP fluorescence, Ca^{2+} imaging and Western blotting.

Cell culture and transient transfection of HEK293 cells

HEK293 cells and HEK293 cells, which stably express either mouse Myc-TRPM3α2-eYFP (6), or mouse YFP-TRPM3α5 (see above) were maintained at 37 °C in a humidified atmosphere with 5 % CO_2, split each week two or three times and replaced from time to time from frozen stocks in order to maintain the passage

number below 40. To the culture medium of stably transfected cells, geneticin (0.5 mg / ml, Sigma-Aldrich) was added. For transient transfection of HEK293 cells, PolyFect (Qiagen, Hilden, Germany) was used as recommended by the manufacturer. In particular, we transiently transfected into HEK293 cells: splice variants of mouse TRPM3 (5, 6) in pCAGGS vectors, which possess an IRES-GFP cassette for bicistronic expression of eGFP (Fig. 1 *A* and *C* and *SI Appendix*, Fig. S2 *A* and *B*).

We further transfected splice variants of mouse TRPM3 N-terminally tagged with a triple FLAG tag (Fig. 1*B* and *SI Appendix*, Fig. S2 *C–H*), truncated TRPM3α2 and TRPM3α5 constructs (*SI Appendix*, Fig. S1), mouse TRPM3α2-YFP and its mutants in the region encoded by exon 17 (and surroundings) in pcDNA3 (Fig. 2 and *SI Appendix*, Fig. S6), human $G\beta_1$ (in pCMV, a kind gift of Dr. Moritz Bünemann, Marburg, Germany; Fig. 1*C* and *SI Appendix*, Fig. S2*B*) and $G\gamma_2$ (in pcDNA3, a kind gift of Dr. Mike Zhu, Dallas, Texas; Fig. 1*C*, Fig. 4*C*, *SI Appendix*, Fig. S2*B* and *SI Appendix*, Fig. S7 *B* and *C*), human μOR (in pCAGGS-IRES-GFP; Fig. 1 *A* and *B*; Fig. 2; *SI Appendix*, Fig. S1 *B* and *C*; *SI Appendix*, Fig. S2 *A* and *C–H* and *SI Appendix*, Fig. S6), human Myc-$G\beta_1$ and its mutants in pcDNA3 (Fig. 4*C* and *SI Appendix*, Fig. S7 *B* and *C*).

Functional studies on HEK293 cells

Ca^{2+} imaging and whole-cell patch-clamp electrophysiology was performed as described (4, 9, 10).

Ca^{2+} imaging: Poly-L-lysine-coated (MW: 70,000; Sigma-Aldrich) glass cover slips with the adherent cells attached were incubated with 5 μM Fura2-AM (Biotrend, Cologne, Germany) for 30 min. in culture medium at room temperature. Subsequently, cover slips were attached to a closed recording chamber (Warner Instruments, Hamden, CT, USA) and continuously superfused with standard extracellular solution using a gravity-driven perfusion system. For the application of pharmacological substances, solution exchange was realized with a gravity-driven perfusion system controlled by a valve bench (ALA Scientific Instruments, Farmingdale, New York, USA) leading to a manifold close to the inlet of the recording chamber. During the measurement, an image pair was taken every 5 s at 510 nm with an HQ_2 camera (Photometrics, Tucson, Arizona, USA) during alternating excitation at 340 and 380 nm using an inverted microscope (Nikon, Düsseldorf, Germany) equipped with a 10x SFluor objective (N.A. 0.5). From a fluorescence image with 380 nm excitation or a fluorescence image of the GFP/YFP fluorescence, regions of interest representing each a single cell were selected manually. Ratio images were calculated with MicroManager (11), using a custom-written plugin after background subtraction and thresholding. Ratio data were averaged over all pixels of a single cell (as defined by the thresholded ROI) and single cell traces were analyzed off-line for cells that responded to pregnenolone sulfate stimulation with an increase in ratio values larger than 0.05 or 0.1, depending on the specific

experiment. μOR-mediated inhibition was calculated by subtracting the baseline fluorescence, and measuring the pregnenolone sulfate-induced ratio increase before (R_{before}), during (R_{during}) and after (R_{after}) DAMGO application (by averaging the last 5 data points). Inhibition (*Inh*, expressed in %) was calculated as:
$Inh = 100 - (100 * R_{during} / ((R_{before} + R_{after}) / 2))$
For quantifying the reduction in TRPM3 activity due to overexpression of Gβγ proteins (Figs 1*C* and 4*C*, *SI Appendix*, Fig. S2*B*, *SI Appendix*, Fig. S7*B*), the baseline subtracted pregnenolone sulfate-induced increase of the ratio values (Δratio) is reported for individual cells together with the descriptive statistics.

Whole-cell patch-clamp electrophysiology: Offset potentials were nullified before reaching the cell-attached configuration and series resistances were compensated (typically by 80 %). Potential values reported in this paper have been corrected offline for the calculated liquid junction potential of 15 mV. Voltage ramps (1 mV / ms) from −115 to +85 mV were applied at a frequency of 0.5 or 1 per second. A holding potential of −15 mV was used between the ramps. Solution exchange was obtained with the help of a valve bench as described above for Ca^{2+} imaging experiments. The solution was exchanged locally in the vicinity of the recorded cell by using a custom-made miniature manifold, connected to a small (inner diameter 320 μm) outlet that was placed at a distance of approx. 200 – 300 μm from the patched cell. For graphs showing the current over time, the current values measured during the voltage ramps at −80 and +80 mV were extracted offline. μOR-induced inhibition (*Inh*, in %) was calculated from current values obtained at −80 and +80 mV separately, as:
$Inh = 100 – (100 * I_{DAMGO} / I_{PS})$,
where I_{DAMGO} is the baseline-subtracted current during the application of DAMGO and pregnenolone sulfate and I_{PS} is the baseline-subtracted current during the initial pregnenolone sulfate application.

Solutions: The extracellular solution for Ca^{2+} imaging and patch-clamp experiments contained (in mM): 145 – 149 NaCl, 10 CsCl, 3 KCl, 2 $CaCl_2$, 2 $MgCl_2$, 10 HEPES, 10 D-glucose. Sometimes 10 mM D-glucose was substituted by 3 mM D-glucose and 7 mM D-mannitol. These solutions were always adjusted with NaOH to pH 7.2. The osmolality was established to 315 – 335 mOsm / kg by the addition of D-glucose or H_2O. The intracellular solution for patch-clamp experiments contained (in mM): 140 – 145 CsOH, 10 BAPTA, 50 CsCl, 80 aspartate, 4 Na_2ATP, 3 $MgCl_2$, 10 HEPES. The pH was adjusted to 7.2 with CsOH and the osmolality of this solution was in the range of 285 – 315 mOsm / kg. The concentrations indicated in this section are the final values after adjustment of pH and osmolality. Pregnenolone sulfate was obtained from Steraloids (Newport, Rhode Island, USA) or Sigma-Aldrich and dissolved in DMSO at a stock concentration of 50 mM. DAMGO ([D-Ala2, N-Me-Phe4, Gly5-ol]-enkephalin acetate), was purchased from

Sigma-Aldrich and also prepared as a stock solution in DMSO (2 mM). In the final solutions applied to the cells, the concentration of DMSO did not exceed 0.25 %.

Electrophysiology of Xenopus laevis *oocytes*

Two-electrode voltage clamp (TEVC) measurements of *Xenopus laevis* oocytes were performed as described earlier (12). Animal procedures for the work with *Xenopus laevis* frogs were approved by the Institutional Animal Care and Use Committee at Rutgers New Jersey Medical School. For *Xenopus laevis* oocyte preparations frogs were anesthetized in 0.25 % ethyl 3-aminobenzoate methanesulfonate solution (MS222, Tricaine-methanesulfonate, Western Chemical Inc, Ferndale, Washington, USA) in H_2O (pH 7.4). Ovaries were removed from the anesthetized frogs and were digested overnight at 16 °C in 0.1 – 0.2 mg / ml type 1A collagenase (Sigma-Aldrich), in OR2 solution containing 82.5 mM NaCl, 2 mM KCl, 1 mM $MgCl_2$ and 5 mM HEPES (pH 7.4). The next day the oocytes were washed multiple times with OR2 solution, then placed in OR2 solution supplemented with 1.8 mM $CaCl_2$ and 100 IU / ml penicillin and 100 mg / ml streptomycin and kept in a 16 °C incubator. cRNA (30 – 35 ng) transcribed from the linearized human TRPM3 cDNA clone (13) in the pGEMSH vector and from $G\beta_1$ and $G\gamma_2$ (1 ng each) or $G\beta_1$ mutants (1 ng) were microinjected into individual oocytes. The injection was carried out with a nanoliter-injector system (Warner Instruments, Hamden, Connecticut, USA). Oocytes were used for electrophysiological measurements 2 – 3 days after microinjection.

Oocytes were placed in a solution containing 97 mM NaCl, 2 mM KCl, 1 mM $MgCl_2$ and 5 mM HEPES, pH 7.4, and currents were recorded with thin-wall inner-filament-containing glass pipettes (World Precision Instruments, Sarasota, Florida, USA) filled with 3 M KCl in 1 % agarose. Currents were recorded with a −100 to +100 mV voltage ramp protocol applied every second (0.25 mV / ms); holding potential was 0 mV using a GeneClamp 500B amplifier and analyzed with the pClamp 9.0 software (Molecular Devices, San José, California, USA). To be able to compare data from experiments in different days, we normalized data from each day to the average pregnenolone sulfate-induced current amplitudes in control TRPM3 expressing oocytes on the same day. $G\beta_1$ mutants were tested in groups of 3 or 4, and experiments were performed on oocytes obtained from 2 – 3 different digestions for each group. As the inhibition levels by $G\beta_1\gamma_2$ showed slight variations between experiments, the data are plotted in the groups in which each mutant was tested (Fig. 4*B*, *SI Appendix*, Fig. S7*A*).

Coimmunoprecipitation experiments

Immunoprecipitations and Western blots were essentially performed as described previously (4). Nontransfected HEK293 cells and HEK293 cells stably expressing mouse Myc-TRPM3α2-YFP (6) or mouse YFP-TRPM3α5 (see above) were solubilized in lysis buffer containing 25 mM Tris (pH 8), 0.5 % (w/v) Triton X-100, 0.5 % (w/v) Na^+-deoxycholate, 50 mM NaCl and a protease inhibitor mix (1 mM phenylmethanesulfonyl fluoride, 1 µg / ml pepstatin, 5 µg / ml leupeptin, 5 µg / ml antipain, 1 µg / ml aprotinin, and 100 µg / ml trypsin inhibitor, Carl Roth, Karlsruhe, Germany, ref. 14). Debris and nuclei were removed by centrifugation, the remaining supernatants were mixed with GFP-Trap agarose beads (ChromoTek, Planegg-Martinsried, Germany) and kept moving at 4 °C over night. Afterwards, beads were washed once with lysis buffer and four times with binding buffer containing 20 mM HEPES (pH 7.4), 0.01 % (w/v) CHAPS, 140 mM K^+ aspartate, 5 mM $MgCl_2$, 10 mM EGTA and 0.04 mM dithiothreitol (15). Following SDS-PAGE and protein transfer to nitrocellulose membranes (GE Healthcare, Solingen, Germany) fluorescence (Odyssey Sa, LI-COR Biosciences, Bad Homburg, Germany) or chemiluminescence (ChemoCam Imager, Intas, Göttingen, Germany) detection systems were used together with the following antibodies: anti-GFP (Santa Cruz, sc-8334, 1:500), anti-Gβ (Santa Cruz, sc-378, 1:500), anti-rabbit IgG-IRDye-800CW (LI-COR, #926–32211, 1:10,000), anti-mouse IgG-HRP (Santa Cruz, sc-2031, 1:10,000), anti-rabbit IgG-HRP (Santa Cruz, sc-2030, 1:10,000). After densitometric quantification using ImageJ (16, 17) and background subtraction, the density values for the coimmunoprecipitated Gβ proteins were normalized to the density values obtained for Gβ immunoprecipitated with TRPM3α2 (*SI Appendix*, Fig. S5 *B* and *C*) or, after additional subtraction of the Gβ density values from nontransfected control cells, normalized to the density values of the immunoprecipitated TRPM3 proteins (*SI Appendix*, Fig. S5 *D* and *E*).

Western blotting

For the estimation of the expression levels of mutated Myc-$Gβ_1$, transiently transfected HEK293 cells were solubilized with lysis buffer as described above (section “Coimmunoprecipitation experiments”) two days after transfection. After removal of debris and nuclei by centrifugation at 13,000 x g the protein concentrations of the remaining supernatants were determined with Roti-Quant (Carl Roth) according to the manufacturer's instructions. Equal protein amounts were loaded onto SDS-polyacrylamide gels and separated by SDS-PAGE. After transfer to nitrocellulose membranes, Myc-$Gβ_1$ proteins and endogenous early endosomal antigen 1 (EEA1) proteins (loading control) were visualized with anti-c-myc antibodies (Roche, Mannheim, Ger-

many, clone 9E10, 1:1500), anti-EEA1 antibodies (Dianova, Hamburg, Germany, 1:1000) and a chemiluminescence detection kit (SuperSignal Femto, Thermo Fisher, Karlruhe, Germany).

Cocrystallization of $G\beta_1\gamma_2$(C68S) with a peptide encoded by TRPM3 exon 17

A peptide corresponding to the murine TRPM3 region encoded by exon 17 and surrounding residues (amino acid sequence KRPKALKLLGMEDDI, exon 17-encoded amino acids are underlined) was obtained from Genscript (Leiden, The Netherlands) as lyophilized trifluoroacetic acid (TFA) salt with a HPLC purity of 97.7 %. It was dissolved in H_2O at a concentration of 10 mg / ml (according to the total peptide mass stated by Genscript). For crystallization, a mixture of purified Gβγ(C68S) with a concentration of 140 µM and TRPM3 peptide with a concentration of 280 µM was prepared (around 100 µl 6.7 mg / ml Gβγ(C68S) + 5 µl peptide stock solution) and incubated on ice for 1 h. Initial crystallization plates in commercially available screens were set up with 0.2 µl (complex solution) + 0.2 µl (reservoir) drops using the Mosquito crystal robot (TTP Labtech, Melbourn, UK). After two days incubating at 18 °C, in Hampton Crystal Screen condition 41 (0.1 M HEPES sodium pH 7.5, 20 % (w/v) polyethylene glycol 4,000, 10 % (v/v) isopropanol) a cluster of thin needles appeared. This cluster was used to prepare a crystal seed stock by crushing the crystals into small pieces and adding 50 µl mother liquor solution (50 % size exclusion buffer from Gβγ(C68S) purification, 50 % reservoir solution). For reasons of reproducibility the seed stock was aliquoted into several tubes, flash frozen in liquid nitrogen and stored at −80 °C before further use. A fresh aliquot was thawed to prepare a 10-fold dilution series of seeds in mother liquor. A new crystallization plate with 0.2 µl (complex solution) + 0.2 µl (Hampton Crystal Screen condition 41 replicate) + 0.04 µl (seeds in different dilutions) drops was set up to find an appropriate seed dilution (around 2 to 3 needle clusters per well on average). The determined seed dilution was then used in further grid screening optimizations of the crystallization condition, using a freshly thawed seed stock aliquot. The best diffracting single 3D crystals grew in 0.1 M HEPES sodium pH 7.5, 15 % (w/v) polyethylene glycol 4,000, 7.5 % (v/v) isopropanol as 0.2 µl + 0.2 µl + 0.04 µl (as before) drops. For crystal freezing, mother liquor solutions of this condition with increasing glycerol concentrations (0 to 25 % in 5 % increments) were prepared and used one after the other to replace the crystal mother liquor, before fishing the crystal with a nylon loop of appropriate size and vitrifying it in liquid nitrogen.

X-ray data collection, structure building and refinement

Diffraction data to 1.94 Å resolution were collected at European Synchrotron Radiation Facility (ESRF) beamline ID30B on a Pilatus detector using a wavelength of 0.9754 Å. Data processing was done in XDS

(18) and Aimless from the CCP4 package (19). Initial phases were determined by molecular replacement using the CCP4 tool Phaser (20) with a prepared Gβγ model from the PDB 1XHM (21), in which the bound peptide and all other non-Gβγ atoms were deleted. Structure building and refinement were done in Coot (22) and REFMAC (23). A final refinement step was done with PDB-REDO (24), yielding R_{work} / R_{free} values of 18.8 % and 22.4 % (*SI Appendix*, Table S1). The final model contains residues 4 to 340 of Gβ, 7 to 68 of Gγ(C68S) and 1 to 13 of the TRPM3 exon 17 peptide. A composite omit map for the full structure using simulated annealing was created with Phenix (25) for unbiased proof of electron density, especially in the region where the peptide is bound (*SI Appendix*, Fig. S11).

Ni^{2+} column pull-down binding experiments

Two samples of 75 µl purified His-tagged maltose-binding protein with C-terminally linked TRPM3 exon 17 peptide (construct as described in section "Expression and purification of TRPM3 exon 17-encoded peptide fused to His-tagged maltose-binding protein") at a concentration of 250 µM were mixed with either 25 µl PBS or 25 µl PBS containing 25 units thrombin (Merck) and incubated over night at 4 °C. 50 µl of purified Gβγ(C68S) (not His-tagged) at a concentration of 75 µM was then added to both samples, which were further incubated for 1 h. 4 µl of each sample were saved for SDS-PAGE. The remaining 146 µl of both samples were loaded on columns containing 250 µl Ni^{2+} Sepharose 6 Fast Flow beads (GE Healthcare), each, which had been pre-incubated with wash buffer, corresponding to the final size exclusion buffer from the Gβγ(C68S) purification including 10 mM imidazole. The immediate flow-through was discarded, as no protein should be expected here, and the Ni^{2+} beads were incubated sitting in the columns without any excess liquid for 1 h at 4 °C. Then, 3x 500 µl of wash buffer were added to both columns and the whole flow-through was collected. Finally, 3x 500 µl of elution buffer, corresponding to wash buffer including 300 mM imidazole, were added to the beads to elute the bound protein and the whole elution was collected.

For SDS-PAGE analysis, the saved 4 µl from the input samples were diluted with wash buffer to 50 µl. In order to keep the concentrations of protein in the wash and elution samples quantifiable and account for the differences in volumes (146 µl loaded on beads, 1500 µl in both the wash and elution from beads), 1500 µl / 146 µl x 4 µl = 41.1 µl of both the wash and elution samples were diluted to 50 µl with wash buffer. To each of these SDS-PAGE samples 25 µl of 3x SDS loading buffer were added and then for each sample 18.75 µl (which contain the equivalent of 1 µl of original input sample for the Ni^{2+} beads) were loaded and analyzed on SDS-PAA-gels (Bio-Rad, Temse, Belgium). The Coomassie-stained gels were scanned and the band intensities were quantified using ImageJ (16, 17).

Bio-layer interferometry (BLI) binding experiments

A peptide corresponding to the TRPM3 region encoded by exon 17 and surrounding residues with an additional N-terminal biotin group and a 6-aminohexanoic acid (Ahx) linker in between (biotin–Ahx–KRPKALKLLGMEDDI, exon 17-encoded residues underlined) was obtained from Genscript as lyophilized TFA salt with a HPLC purity of 95.2 %. It was dissolved in BLI buffer (20 mM Tris pH 7.5, 150 mM NaCl, 5 mM TCEP, 0.05 % TWEEN 20) at a concentration of 1 mM (according to the total peptide mass stated by Genscript). For the bio-layer interferometry binding experiments with the Octet RED96 instrument (PALL FortéBio, Fremont, California, USA), this stock solution was freshly diluted 1:2,000 in the same buffer to obtain a total peptide concentration of 500 nM. Accordingly, a stock solution of the nonbiotinylated version of the peptide at 1 mM was prepared in BLI buffer.

On the other hand, the quadruple mutant peptide KRPAALKAAKMEDDI ($K_{595}A + L_{599}A + L_{600}A + G_{601}K$; used for the control experiments, *SI Appendix*, Fig. S3 *J* and *K*) was synthesized in-house using an Intavis Multipep RSi solid phase peptide synthesis robot (N-terminally acetylated and C-terminally amidated form). Peptide purity (>90%) was evaluated using RP-HPLC purification protocol and the peptide was stored as ether precipitate (−20 °C). For competition experiments, the peptide was dried using nitrogen flow, re-suspended and filtered through 0.2-µm PVDF filters. Stocks were then diluted to the appropriate peptide concentration (up to 100 µM) in BLI buffer.

Streptavidin biosensors were used for the experiments and equilibrated in BLI buffer for at least 10 min. before starting the binding protocol at room temperature consisting of the following steps: (1) baseline in BLI buffer for 60 s; (2) immobilization of the biotinylated peptide at 500 nM concentration for 80 s; (3) wash in BLI buffer for 150 s; (4) baseline in BLI buffer for 60 s; (5) association in BLI buffer with a defined concentration of Gβγ(C68S), as determined with a NanoDrop 2000 (Thermo Scientific, Waltham, Massachusetts, USA), and for competition experiments additionally the nonbiotinylated peptide at defined concentrations, for 200 s; (6) dissociation in the same BLI buffer as the baseline step before association for 300 s. For each association condition control measurements were done with new naked sensors, for which the immobilization step was replaced by an additional wash step in BLI buffer. To account for signal artifacts due to differences in buffers (as e.g. arising from high protein concentrations), from the raw signals of each sensor with immobilized peptide the respective naked control sensor signals were subtracted, which were low in comparison and not indicative of unspecific binding of Gβγ(C68S) to the streptavidin sensor. To determine the K_D of the steady-state analysis of the BLI experiments, the average signals of three technical repeats after reaching the

equilibrium for the different Gβγ(C68S) concentrations (averaged over 10 s) were plotted against the respective concentrations. The data points were fitted assuming a 1:1 binding model with the formula:
$Y = Y_{max} * X / (K_D + X)$,
where X is the protein concentration, Y the signal, Y_{max} the signal at saturation and K_D the dissociation constant represented by the concentration at half saturation of the signal. Calculated values are given as averages of 3 measurements including standard deviations.

Circular dichroism spectroscopy

To analyze the secondary structure content of the nonbiotinylated TRPM3 peptide in solution, it was dissolved at a concentration of 0.2 mg / ml in 150 mM NaCl with 20 mM Tris (pH 7.5). The circular dichroism (CD) measurements were performed at room temperature on a J-1500 CD spectro-photometer (Jasco, Tokyo, Japan). Signals were recorded between 195 nm and 260 nm with 1 nm intervals in five technical repeats and averaged. Background signals of the buffer only with the same settings were subtracted from the obtained data. The predicted CD spectrum of the TRPM3-encoded peptide bound to Gβγ was calculated with PDB2CD (26) using the SP175 (soluble) database. For this purpose all atoms that do not belong to the TRPM3 peptide were deleted from the coordinates of the cocrystal structure.

Statistics

Ca^{2+} imaging experiments are represented as mean +/− S.E.M. values from individually recorded cells (numbers indicated in figures). Electrophysiologically measured traces (Fig. 1*B*, Fig. 4*A* and *SI Appendix*, Fig. S2 *C–G*) represent exemplary experiments, but the associated statistics represent the indicated number of independently repeated experiments. Throughout this manuscript, bar graphs depict mean +/− S.E.M. values, but error bars in *SI Appendix*, Fig. S3*E* represent S.D. values. Statistical testing was done with Graphpad Prism (version 3.02) or Microcal Origin 2019 using ANOVA and Tukey's post-hoc test (Fig. 4*B*), one sample t-test (*SI Appendix*, Fig. S2*A*), Mann-Whitney test (*SI Appendix*, Fig. S2*B* and Fig. S7*B*) and two-tailed paired Student's t-test (*SI Appendix*, Fig. S3*C* and Fig. S5 *C* and *E*). In all figures, * represents $p < 0.05$, ** $p < 0.01$, *** $p < 0.001$ and n.s., meaning "not significant", indicates $p \geq 0.05$.

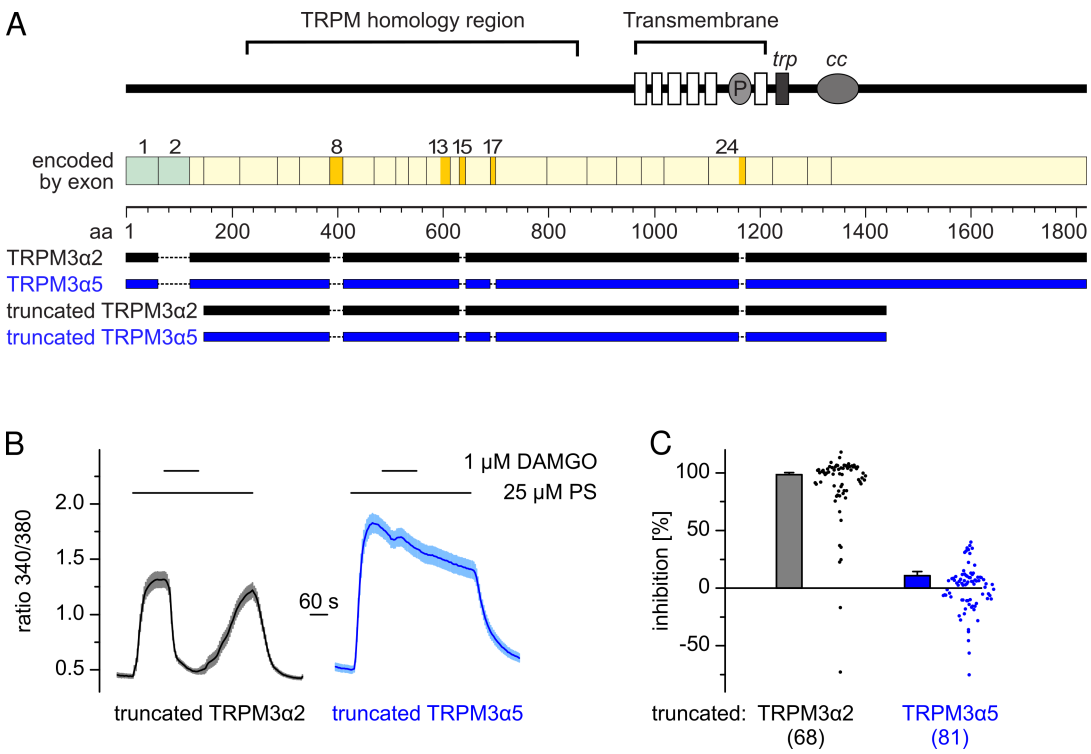

Fig. S1. Interaction between Gβγ and TRPM3 occurs N-terminally to the transmembrane domains of TRPM3. (*A*) Schematic representation of the truncated versions of TRPM3α2 and TRPM3α5 (compare to Fig. 1*D*, P: pore region, trp: TRP-box, cc: coiled-coil domain). These constructs start with amino acid C_{89} and end with P_{1330} (numbering relative to full-length TRPM3α2). (*B*) and (*C*) Ca^{2+} imaging experiments of cells cotransfected with μORs and one of the truncated TRPM3 constructs show results essentially indistinguishable from experiments with the corresponding full-length TRPM3 proteins (compare to Fig.1*A* and *SI Appendix*, Fig. S2*A*). In particular, truncated TRPM3α2 channels are still strongly inhibited by μOR activation. Numbers in parentheses in *C* indicate the number of cells analyzed.

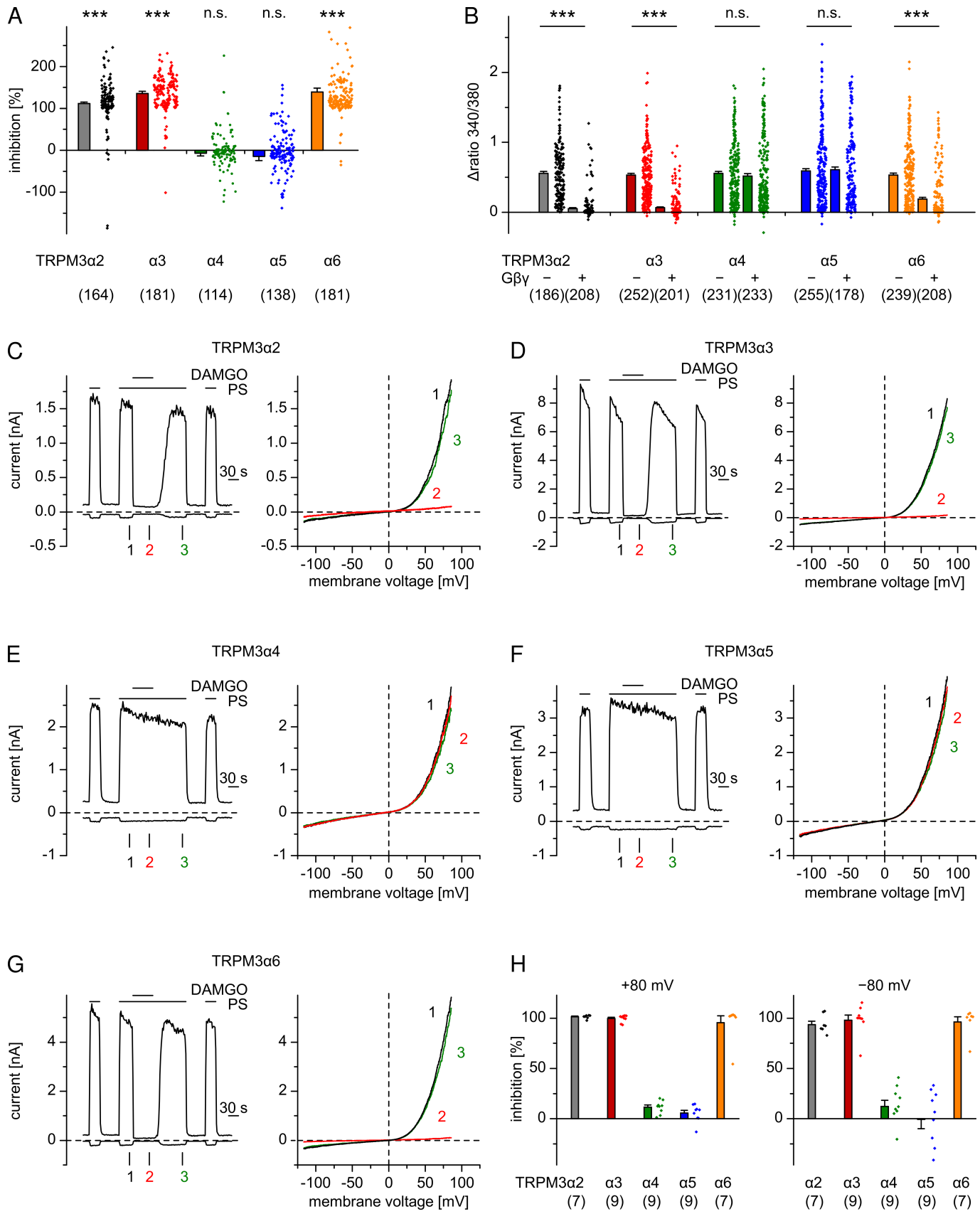
A
***
***
n.s.
n.s.
***
inhibition [%]
200
100
0
-100
TRPM3α2
α3
α4
α5
α6
(164)
(181)
(114)
(138)
(181)
B
***
***
n.s.
n.s.
***
Δratio 340/380
2
1
0
TRPM3α2
α3
α4
α5
α6
Gβγ − + − + − + − + − +
(186)(208)
(252)(201)
(231)(233)
(255)(178)
(239)(208)
C
TRPM3α2
DAMGO
PS
current [nA]
1.5
1.0
0.5
0.0
-0.5
30 s
1 2 3
membrane voltage [mV]
-100 -50 0 50 100
D
TRPM3α3
DAMGO
PS
current [nA]
8
6
4
2
0
-2
30 s
1 2 3
membrane voltage [mV]
-100 -50 0 50 100
E
TRPM3α4
DAMGO
PS
current [nA]
2
1
0
-1
30 s
1 2 3
membrane voltage [mV]
-100 -50 0 50 100
F
TRPM3α5
DAMGO
PS
current [nA]
3
2
1
0
-1
30 s
1 2 3
membrane voltage [mV]
-100 -50 0 50 100
G
TRPM3α6
DAMGO
PS
current [nA]
4
2
0
30 s
1 2 3
membrane voltage [mV]
-100 -50 0 50 100
H
+80 mV
−80 mV
inhibition [%]
100
50
0
TRPM3α2 α3 α4 α5 α6
(7) (9) (9) (9) (7)
α2 α3 α4 α5 α6
(7) (9) (9) (9) (7)

Fig. S2. Single cell data and statistical analysis of the data shown in Fig. 1. (*A*) Statistical analysis of data shown in Fig. 1*A*. Percentage of inhibition was calculated for each cell individually, each dot to the right of the columns (which represent mean and S.E.M.) represents an individual cell. For each splice variant (except for TRPM3α2), 2 or 3 outliers are not depicted, but were included in the statistical analysis. Asterisks indicate statistical significance for difference from zero (two-sided one sample t-test). (*B*) Statistical analysis of the data in Fig. 1*C*. The conventions are the same as in *A*, the statistical testing was done with a Mann-Whitney test. (*C*) – (*G*) Current-voltage relationship (I/V curves, right-hand panels) for the recordings shown in Fig. 1*B*. Left hand panels show the same recordings as Fig. 1*B*, but also indicate the time points at which the I/V curves were measured. The shapes of the I/V curves of the individual splice variants of TRPM3 are highly similar and the μOR activation by DAMGO (1 μM) suppresses both inward (at −80 mV) and outward (at +80 mV) currents induced by 25 μM PS for the splice variants TRPM3α2, α3 and α6. (*H*) Quantification of the inhibition calculated for single cells and for currents at +80 mV (left hand panel) and −80 mV (right hand panel) separately. The numbers in parentheses in *A*, *B* and *H* indicate the number of cells analyzed.

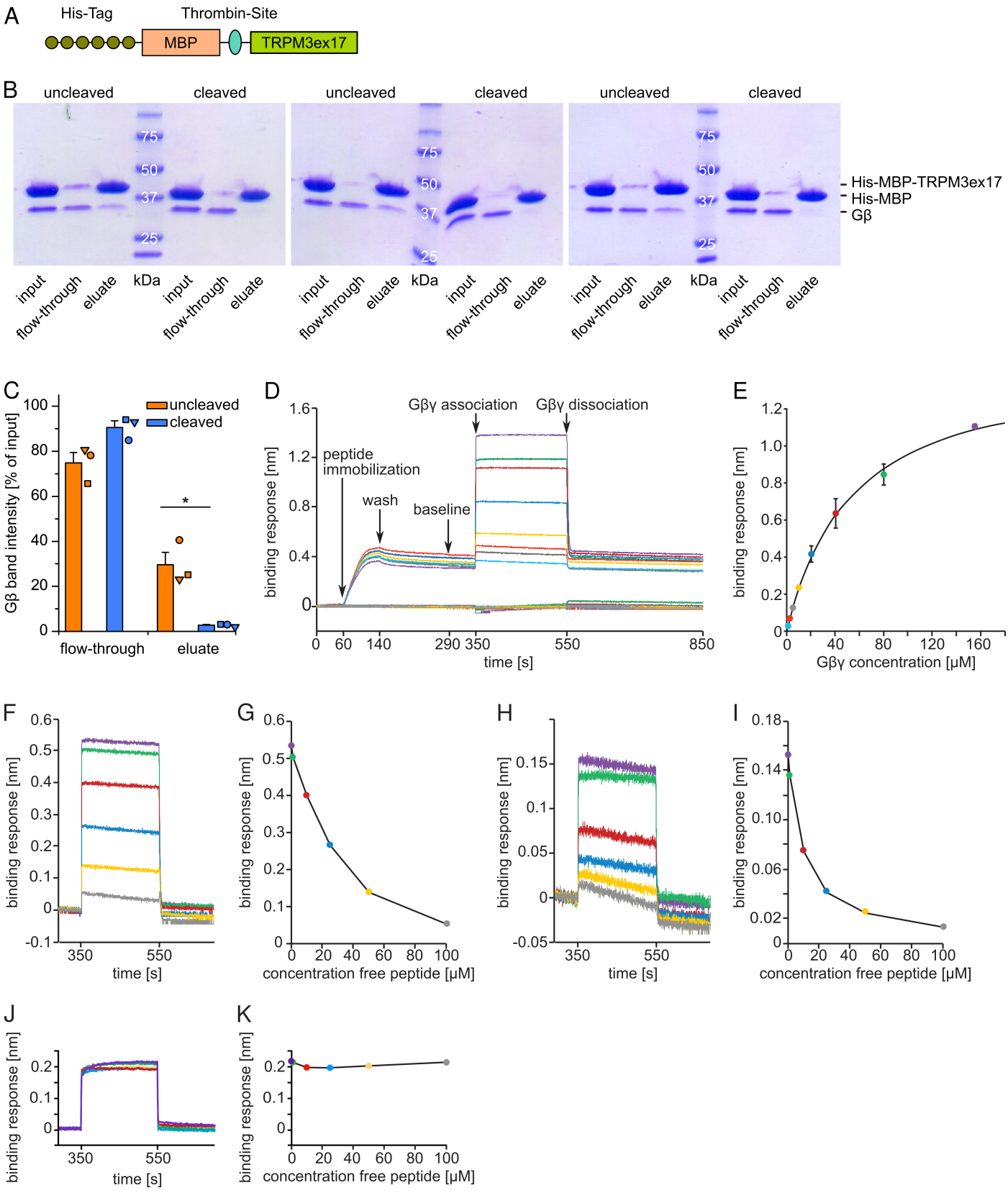
A
His-Tag
Thrombin-Site
MBP
TRPM3ex17
B
uncleaved
cleaved
kDa
input
flow-through
eluate
His-MBP-TRPM3ex17
His-MBP
Gβ
C
Gβ band intensity [% of input]
uncleaved
cleaved
flow-through
eluate
D
Gβγ association
Gβγ dissociation
peptide immobilization
wash
baseline
binding response [nm]
time [s]
E
binding response [nm]
Gβγ concentration [μM]
F
binding response [nm]
time [s]
G
binding response [nm]
concentration free peptide [μM]
H
binding response [nm]
time [s]
I
binding response [nm]
concentration free peptide [μM]
J
binding response [nm]
time [s]
K
binding response [nm]
concentration free peptide [μM]

Fig. S3. A peptide encompassing exon 17-encoded amino acids of TRPM3 directly interacts with Gβγ. (*A*) Schematic representation of the His-tagged maltose-binding protein (MBP) construct, fused to the amino acids encoded by exon 17 of TRPM3. (*B*) Coomassie-stained SDS-PAGE gels showing the bands of the intact construct from *A* (upper band) and Gβ (lower band) in the sample applied on nickel beads (input), not binding to the beads (flow-through) and eluted from the beads with high imidazole concentration (eluate) on the left hand side of the molecular weight marker. On the right hand side of the marker the corresponding samples were first incubated with thrombin to cut off the exon 17-encoded amino acids (leading to a visible reduction in molecular weight), and then treated as the samples on the left hand side. (*C*) Statistical analysis of the Gβ bands from the three pull-down experiments as shown in *B* (paired t-test, $p = 0.037$); each of the three symbols represents an individual experiment. (*D*) and (*E*) Bio-layer interferometry binding analysis between TRPM3 exon 17 peptide and Gβγ. (*D*) Raw data plotted for the full run of one experiment with Gβγ in concentrations of about 155 (purple), 80 (green), 40 (dark red), 20 (dark blue), 10 (yellow), 5 (grey), 2.5 (light red), and 1.25 (light blue) μM, as well as the control naked sensors (with the same Gβγ concentrations in the same colors, lower traces). (*E*) The processed signals for the different Gβγ concentrations from *D*, with the control signals subtracted, as average of all three technical repeats (mean +/− SD). A curve was fitted to the mean values assuming a 1:1 binding model (fitting parameter: K_d of 55.9 ± 12.9 μM, $n = 3$). (*F*) – (*K*) Competitive binding experiments using bio-layer interferometry demonstrating that free peptide competes with biotinylated peptide fixed on the sensor. The concentration of fixed Gβγ was 19.3 μM in *F* and *G* and 4.9 μM in *H* and *I*. In *J*, a mutated peptide was used that differs in four amino acid residues from the original, wild-type peptide. These mutations were designed to minimize the specific binding of the peptide to Gβγ in order to test for unspecific binding events. (*F*), (*H*), (*J*) Traces show association and dissociation of Gβγ (after subtraction of traces from control sensors), with increasing concentrations of soluble peptide at 0 (purple), 1 (green), 10 (red), 25 (light blue), 50 (yellow), and 100 (grey) μM. (*G*), (*I*), (*K*) Steady-state data extracted from *F*, *H* and *J*.

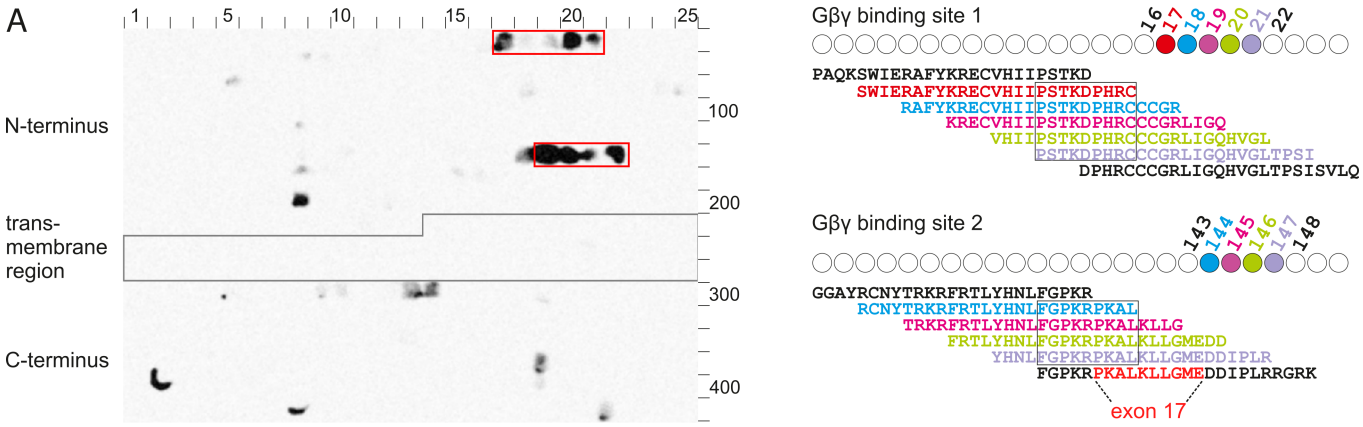
A
N-terminus
trans-membrane region
C-terminus
Gβγ binding site 1
Gβγ binding site 2
exon 17

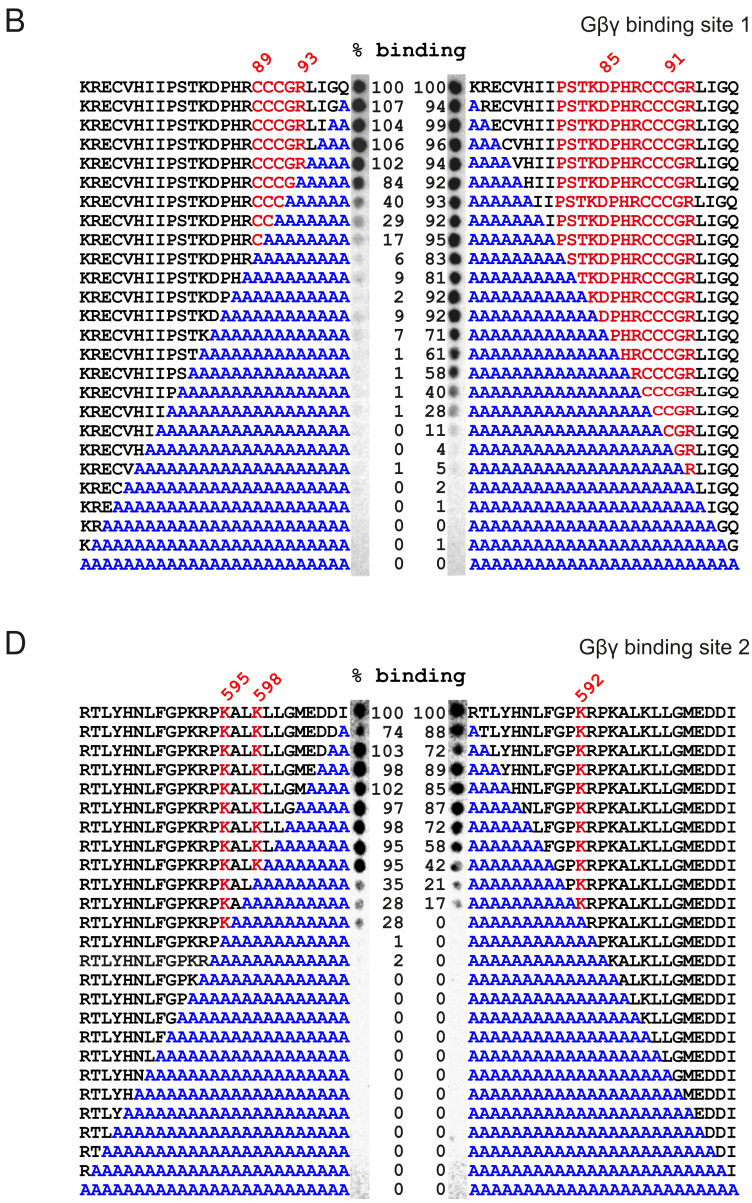
B
Gβγ binding site 1
% binding

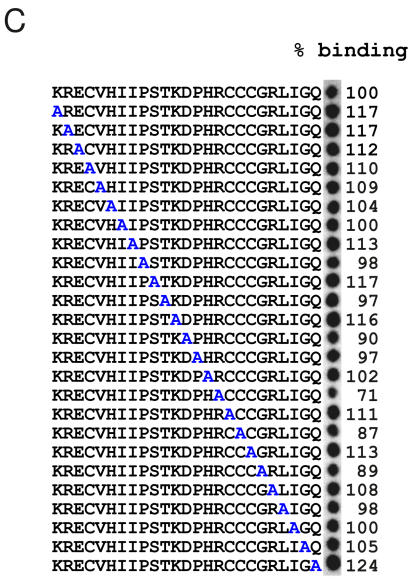
C
% binding

D
Gβγ binding site 2
% binding

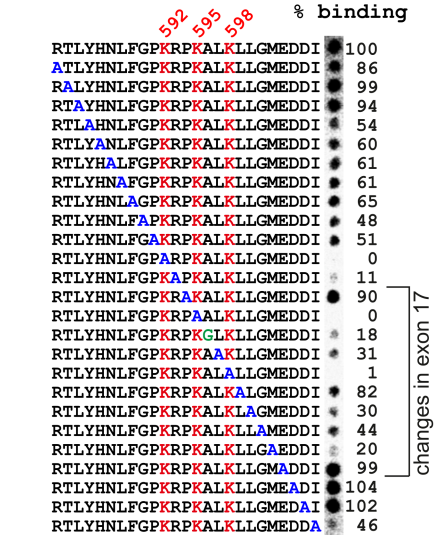
E
% binding
changes in exon 17

Fig. S4. Dot blot analysis of Gβγ binding to TRPM3-derived peptides. (*A*) Binding of purified Gβγ proteins to 422 individual 25-mer peptides spotted on a cellulose membrane and covering the complete TRPM3α2 sequence. The peptides with the most prominent signals (defining Gβγ binding site 1 and 2) are boxed in red (left) and their sequences are indicated in color (right). Common amino acid residues are indicated with a box. (*B*) and (*E*) Identification of amino acid residues essential for Gβγ interaction within binding site 1 (*B* and *C*) and binding site 2 (*D* and *E*). 25-mer polypeptides with progressive replacement by alanine residues starting either at the C-terminus (*B* and *D*, left panels) or at the N-terminus (*B* and *D*, right panels) or with systematic replacement of single amino acid residues within the peptide sequences by alanine (A, highlighted in blue within the sequence) or glycine (G, green) were tested (*C* and *E*). Binding intensities (%) were calculated relative to the signal obtained with the unmodified sequence. Residues most important for Gβγ binding are highlighted in red and their positions within the TRPM3α2 protein are indicated. Note that binding site 2 is near to exon 17-encoded amino acids and contains them partially.

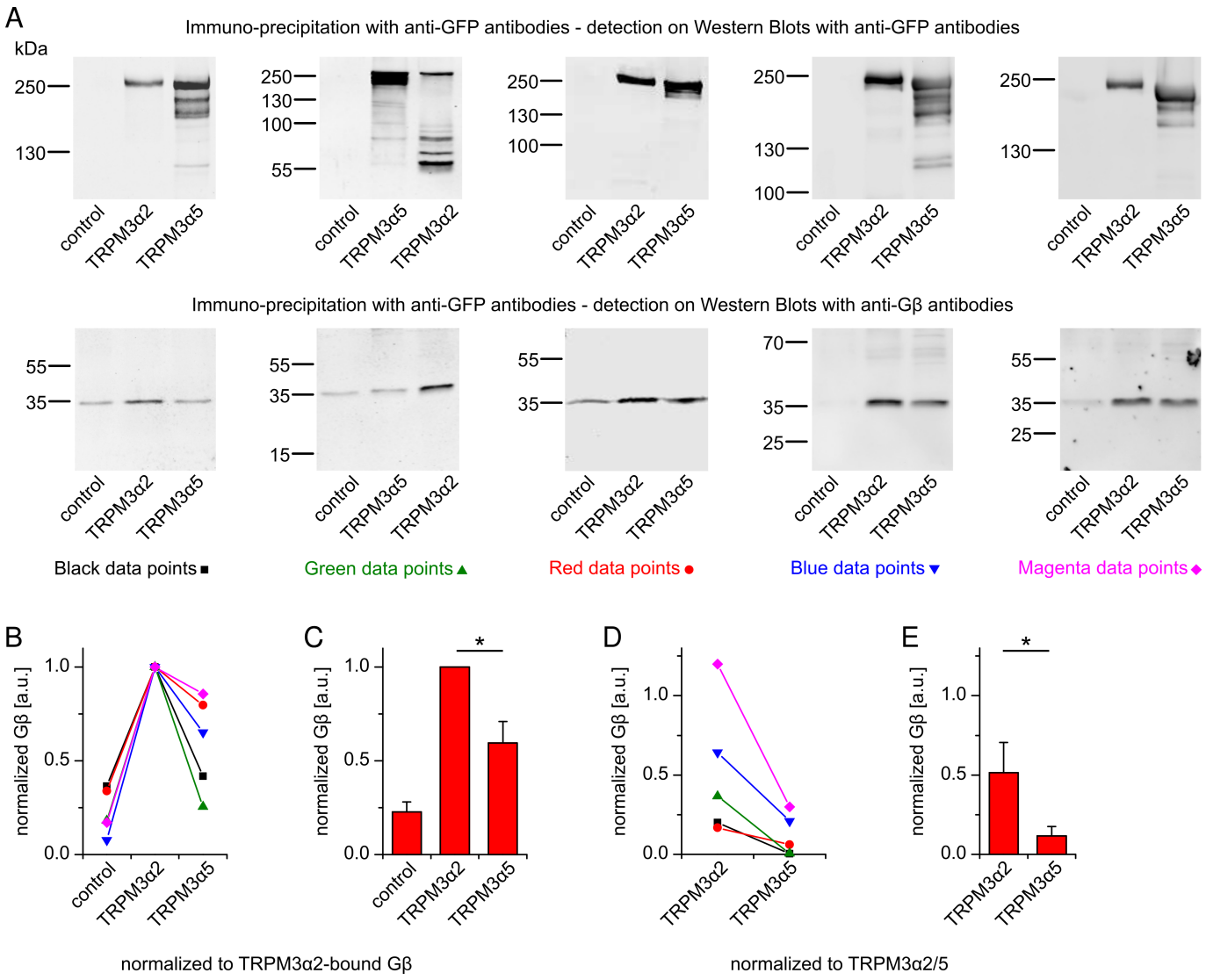

Fig. S5. The interaction of full-length TRPM3 and Gβ proteins is influenced by exon 17. (*A*) Five pairs of Western blots showing coimmunoprecipitation experiments with untransfected HEK293 cells (control) or HEK293 cells stably expressing TRPM3α2 or TRPM3α5 proteins, both fused to YFP. Protein complexes were precipitated with beads coated with anti-GFP antibodies (recognizing the YFP tag) and visualized either using anti-GFP antibodies (upper row) or, on different gels, anti-Gβ antibodies (lower row). The two blots in each column belong to the same experiment. Please note that the order of TRPM3α2 and TRPM3α5 was reversed for the blots in the second column. The color code used in *B* and *D* is indicated. (*B*) Amount of Gβ precipitated in the five individual Western blots shown in *A*, as determined by densitometry. Background-subtracted densitometric values of the lower row blots (anti-Gβ antibodies) were normalized to the value obtained for TRPM3α2-bound Gβ for each blot separately. (*C*) Summary data and statistical analysis (paired t-test, $p = 0.024$) of the densitometric values shown in *B*. The analysis shown in *B* and *C* may have systematically overestimated the relative amount of Gβ coprecipitated with TRPM3α5, since we found that TRPM3α5 proteins were more abundant than TRPM3α2 proteins in the precipitated fraction (*A*, upper row). The analysis shown in *D* and *E* is an attempt to improve this by re-analyzing the data with additional normalizations. (*D*) and (*E*) The binding of endogenously expressed Gβ to the beads coated with anti-GFP antibodies (as seen

in the untransfected “control” lanes) was subtracted from the densitometric data for Gβ on the two other lanes. Additionally, these subtracted values were normalized to the relative abundance of the corresponding TRPM3 proteins (densitometric values obtained from *A*, upper row). This normalization assumes a linear relation between density of the TRPM3 protein bands and the actual amount of TRPM3 protein expressed in the cells. While such a linear model is unlikely to be correct, it may be argued that it gives better results than no correction. (*D*) The correspondingly analyzed and corrected values for the five independent coimmunoprecipitation experiments. (*E*) Summary data and statistical analysis for the re-analyzed data (paired t-test, $p = 0.044$).

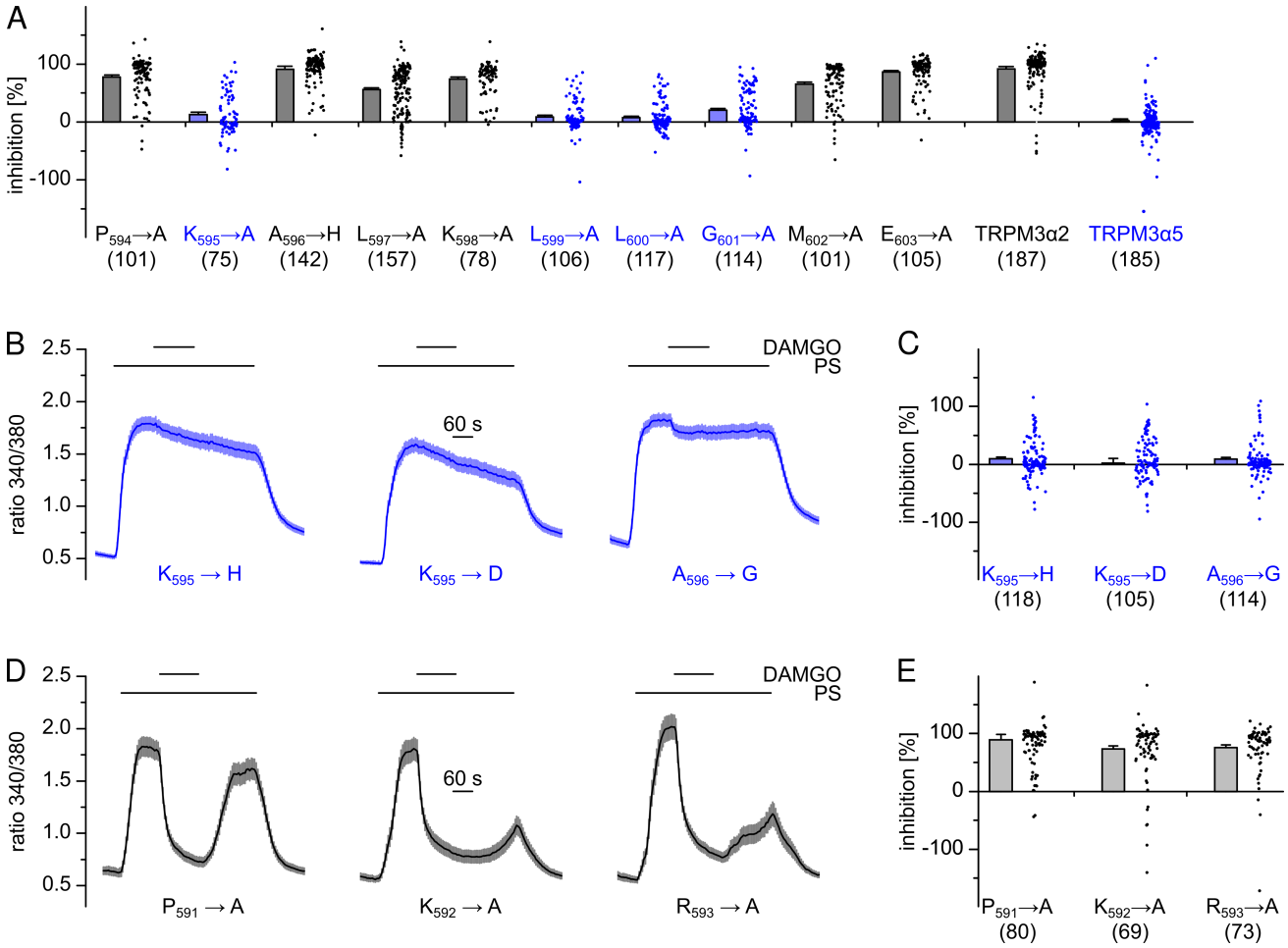

Fig. S6. Single cell analysis of the experiments shown in Fig. 2 and additional point mutations of exon 17-related residues. (*A*) Single cell analysis of data presented in Fig. 2. Additionally, the data from control experiments with wild-type TRPM3α2 and TRPM3α5 are included. The measurements of the A_{596}H mutant, as well as the measurements of TRPM3α2 and TRPM3α5 wild-type, contained 2 cells each for which inhibition values were outside the range displayed. These cells are not shown in the scatter plots, but their values were included in calculating the mean and S.E.M. values. (*B*) – (*E*) Analysis of further mutants in exon 17 (*B* and *C*) and at the C-terminal end of exon 16 (*D* and *E*), performed as in Fig. 2. (*B*) and (*C*) The mutation of the lysine in position 2 of exon 17 (K_{595}) to histidine or aspartate was surprisingly well tolerated and also abolished the μOR-mediated inhibition of the channels. Contrary to the A_{596}H mutation (Fig. 2), the A_{596}G mutation severely affected the μOR-induced inhibition of TRPM3. This may be caused by unusual changes to the overall α-helical structure of the peptide (see Fig. 3) induced by the substitution of alanine to glycine. We did not investigate this mutation further. Measurements for the K_{595}D mutation contained 3 cells and for the A_{596}G mutation 1 cell with inhibition values outside the range displayed in *C*, but their values were included in calculating the mean and S.E.M. values. (*D*) and (*E*) Mutating the last three amino acids of exon 16 individually to alanine did not affect the inhibition of TRPM3 induced by μOR activation. The measurements for the mutation P_{591}A contained two cells with inhibition values outside the range displayed in *E*, that also were included in calculating the descriptive stastistics. Number in parentheses in *A*, *C* and *E* indicate the number of cells analyzed. Throughout this figure, blue indicates mutations or splice variants that did not show channel inhibition after μOR activation.

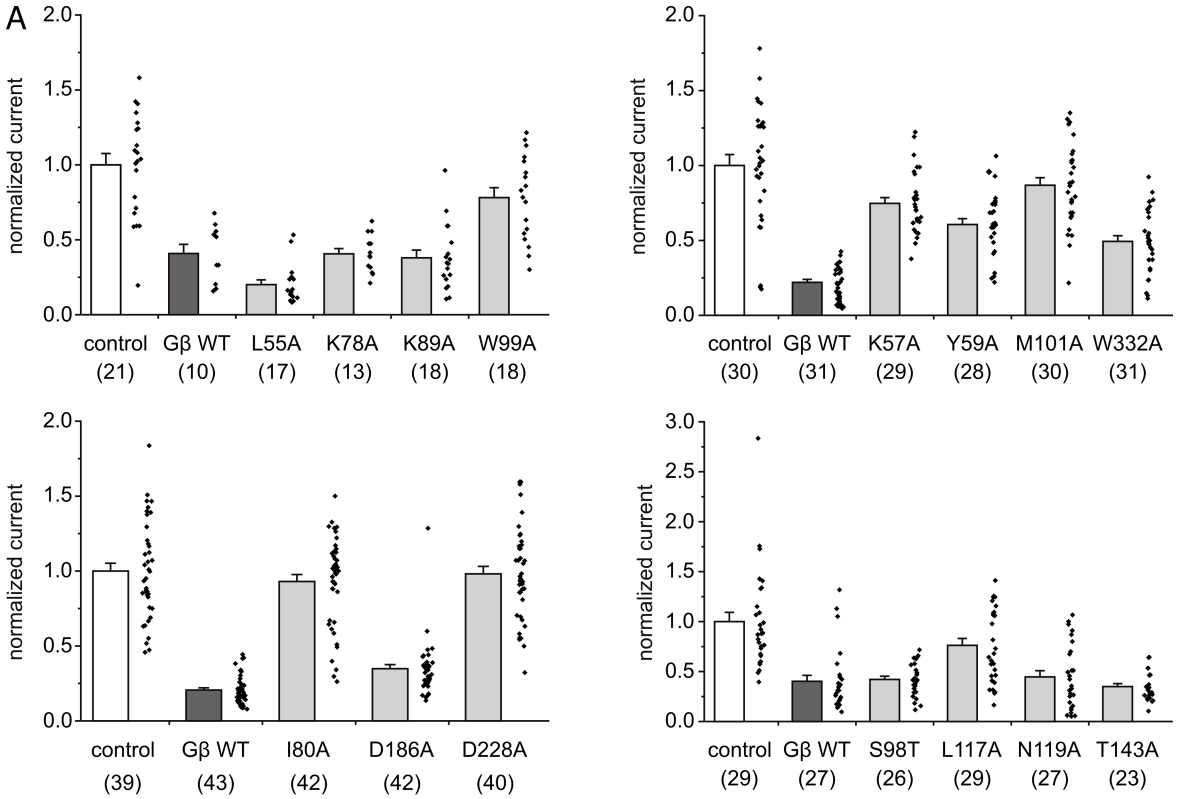
A
normalized current
control (21)
Gβ WT (10)
L55A (17)
K78A (13)
K89A (18)
W99A (18)
control (30)
Gβ WT (31)
K57A (29)
Y59A (28)
M101A (30)
W332A (31)
control (39)
Gβ WT (43)
I80A (42)
D186A (42)
D228A (40)
control (29)
Gβ WT (27)
S98T (26)
L117A (29)
N119A (27)
T143A (23)

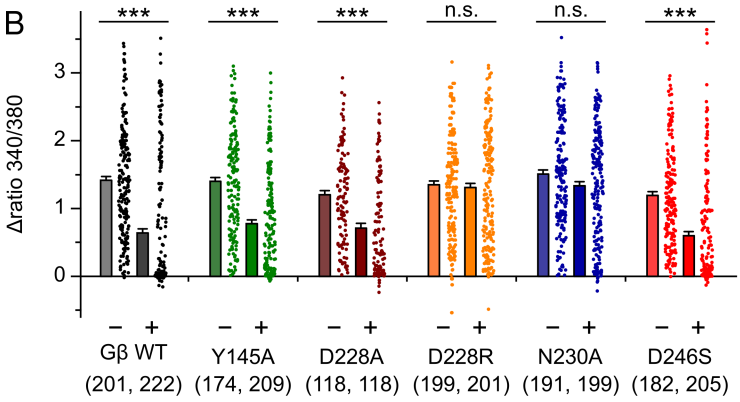
B
Δratio 340/380
***
n.s.
Gβ WT (201, 222)
Y145A (174, 209)
D228A (118, 118)
D228R (199, 201)
N230A (191, 199)
D246S (182, 205)

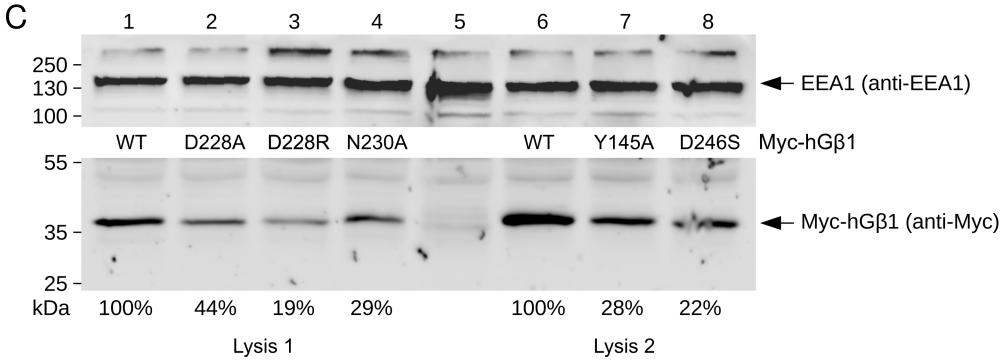
C
1 2 3 4 5 6 7 8
250
130
100
WT D228A D228R N230A WT Y145A D246S Myc-hGβ1
EEA1 (anti-EEA1)
55
35
25
Myc-hGβ1 (anti-Myc)
kDa 100% 44% 19% 29% 100% 28% 22%
Lysis 1
Lysis 2

Fig. S7. Additional data for experiments shown in Fig. 4. (*A*) Single cell data for experiments shown in Fig. 4*B*. **b** Single cell data for data shown in Fig. 4*C*. The bar graphs (showing mean and S.E.M.) in *A* and *B* are identical to those shown in Fig. 4*B* and *C* and are reproduced for convenience. The number of cells analyzed is given for each bar in parentheses. The statistical tests in *B* are Mann-Whitney tests. (*C*)Western blotting of cell lysates and visualization with anti-Myc antibodies showed that all mutants of $G\beta_1$ expressed in HEK293 cells (experiments shown in Fig. 4*C* and in *B*) were expressed, albeit with a reduced expression level. The percentage values indicated are from the densitometric analysis of the Gβ bands and are expressed relative to the expression of wild-type $G\beta_1$.

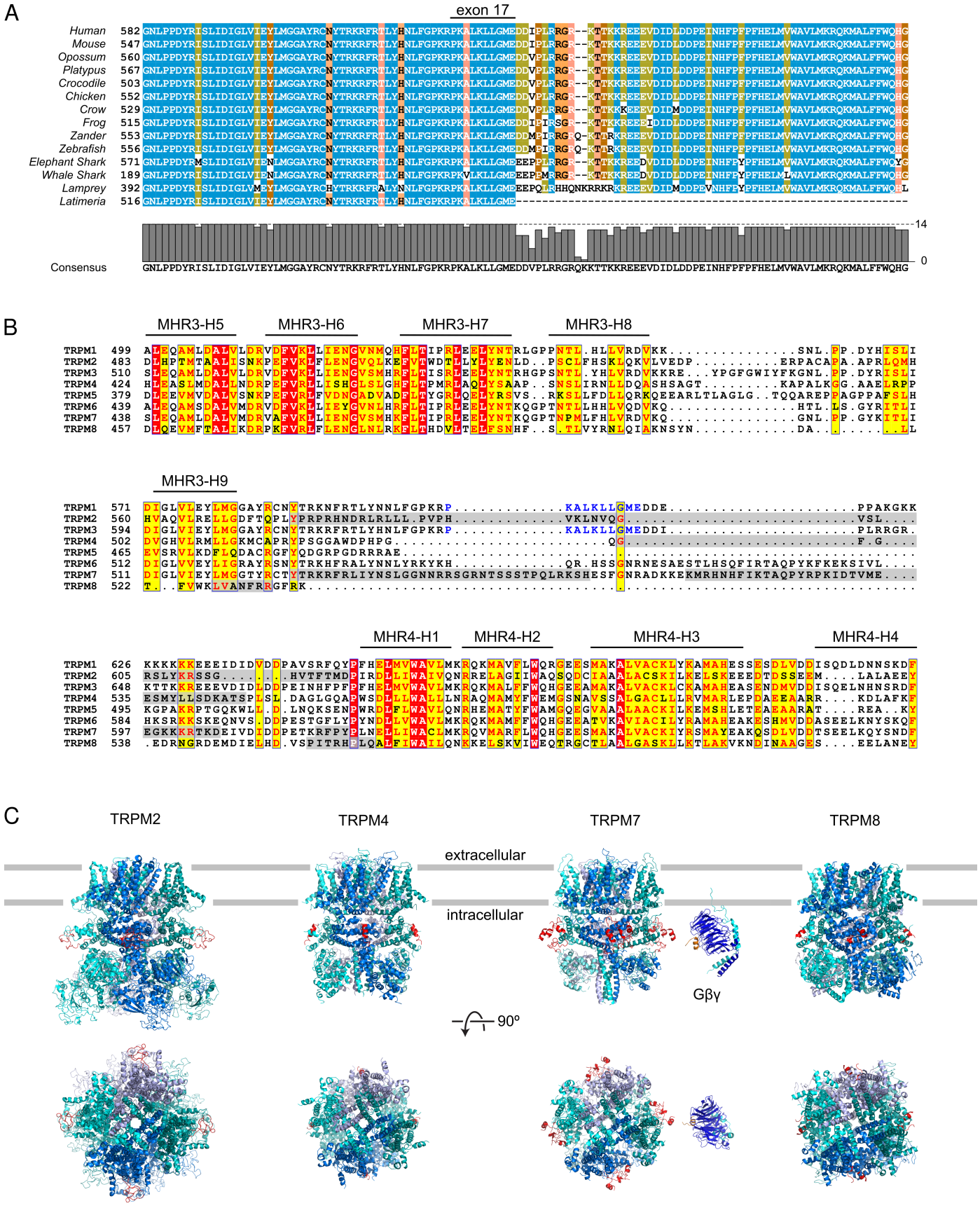
A
exon 17
Human 582 GNLPPDYRISLIDIGLVIEYLMGGAYRCNYTRKRFRTLYHNLFGPKRPKALKLLGMEDDIPLRRGQKTTKKREEEVDIDLDDPEINHFPFPFHELMVWAVLMKRQKMALFFWQHG
Mouse 547 GNLPPDYRISLIDIGLVIEYLMGGAYRCNYTRKRFRTLYHNLFGPKRPKALKLLGMEDDIPLRRGQKTTKKREEEVDIDLDDPEINHFPFPFHELMVWAVLMKRQKMALFFWQHG
Opossum 560 GNLPPDYRISLIDIGLVIEYLMGGAYRCNYTRKRFRTLYHNLFGPKRPKALKLLGMEDDVPLRRGQKTTKKREEEVDIDLDDPEINHFPFPFHELMVWAVLMKRQKMALFFWQHG
Platypus 567 GNLPPDYRISLIDIGLVIEYLMGGAYRCNYTRKRFRTLYHNLFGPKRPKALKLLGMEDDVPLRRGQKTTKKREEEVDIDLDDPEINHFPFPFHELMVWAVLMKRQKMALFFWQHG
Crocodile 503 GNLPPDYRISLIDIGLVIEYLMGGAYRCNYTRKRFRTLYHNLFGPKRPKALKLLGMEDDVPLRRGQKTTKKREEEVDIDLDDPEINHFPFPFHELMVWAVLMKRQKMALFFWQHG
Chicken 552 GNLPPDYRISLIDIGLVIEYLMGGAYRCNYTRKRFRTLYHNLFGPKRPKALKLLGMEDDVPLRRGQKTTKKREEEVDIDLDDPEINHFPFPFHELMVWAVLMKRQKMALFFWQHG
Crow 529 GNLPPDYRISLIDIGLVIEYLMGGAYRCNYTRKRFRTLYHNLFGPKRPKALKLLGMEDDVPLRRGQKTTKKKEEEVDIDMDDPEINHFPFPFHELMVWAVLMKRQKMALFFWQHG
Frog 515 GNLPPDYRISLIDIGLVIEYLMGGAYRCNYTRKRFRTLYHNLFGPKRPKALKLLGMEDDIPIRSGQKTTKKREEEIDIDLDDPEINHFPFPFHELMVWAVLMKRQKMALFFWQHG
Zander 553 GNLPPDYRISLIDIGLVIEYLMGGAYRCNYTRKRFRTLYHNLFGPKRPKALKLLGMEDDMPIRRGQQKTTKKREEEVDIDLDDPEINHFPFPFHELMVWAVLMKRQKMALFFWQHG
Zebrafish 556 GNLPPDYRISLIDIGLVIEYLMGGAYRCNYTRKRFRTLYHNLFGPKRPKALKLLGMEDDMPIRRGQQKTTKKREEEVDIDLDDPEINHFPFPFHELMVWAVLMKRQKMALFFWQHG
Elephant Shark 571 GNLPPDYRMSLIDIGLVIENLMGGAYRCNYTRKRFRTLYHNLFGPKRPKALKLLGMEEEPPLRRGQKTTKKREEDVDIDLDDPEINHFPYPFHELMVWAVLMKRQKMALFFWQYG
Whale Shark 189 GNLPPDYRISLIDIGLVIENLMGGAYRCNYTRKRFRTLYHNLFGPKRPKVLKLLGMEEEPPMRRGQKTTKKREEDVDIDLDDPEINHFPYPFHELMVWAVLMKRQKMALFFWQHG
Lamprey 392 GNLPPDYRISLIDIGLVMEYLMGGAYRCHYTRKRFRALYNNLFGPKRPKALKLLGMEEEPQLFHHQNKRKRKRKREEVDIDMDDPEVNHFPYPFHELMVWAVLMKRQKMALFFWQIL
Latimeria 516 GNLPPDYRISLIDIGLVIEYLMGGAYRCNYTRKRFRTLYHNLFGPKRPKALKLLGME----------
14
0
Consensus GNLPPDYRISLIDIGLVIEYLMGGAYRCNYTRKRFRTLYHNLFGPKRPKALKLLGMEDDVPLRRGQKTTKKREEEVDIDLDDPEINHFPFPFHELMVWAVLMKRQKMALFFWQHG
B
MHR3-H5
MHR3-H6
MHR3-H7
MHR3-H8
TRPM1 499 ALEQAMLDALVLDRVDFVKLLIENGVNMQHFLTIPRLEELYNTRLGPPNTL.HLLVRDVKK.....SNL.PP.DYHISLI
TRPM2 483 DLHPTMTAALISNKPEFVKLFLENGVQLKEFVTWDTLLYLYENLD..PSCLFHSKLQKVLVEDP.....ERPACAPA.APRLQMH
TRPM3 510 SLEQAMLDALVLDRVDFVKLLIENGVSMHRFLTISRLEELYNTRHGPSNTL.YHLVRDVKKRE...YPGFGWIYFKGNL.PP.DYRISLI
TRPM4 424 HLEASLMDALLNDRPEFVRLLISHGLSLGHFLTPMRLAQLYSAAP..SNSLIRNLLDQASHSAGT.....KAPALKGG.AAELRPP
TRPM5 379 DLEEVMVDALVSNKPEFVRLFVDNGADVADFLTYGRLQELYRSVS..RKSLLFDLLQRKQEEARLTLAGLG..TQQAREPPAGPPAFSLH
TRPM6 439 ALEQAMSDALVMDRVDFVKLLIEYGVNLHRFLTIPRLEELYNTKQGPTNTLLHHLVQDVKQ.....HTL.LS.GYRITLI
TRPM7 438 SLEQAMLDALVMDRVAFVKLLIENGVSMHKFLTIPRLEELYNTKQGPTNPMLFHLVRDVKQ.....GNL.PP.GYKITLI
TRPM8 457 DLQEVMFTALIKDRPKFVRLFLENGLNLRKFLTHDVLTEPFSNHF..S.TLVYRNLQIAKNSYN.....DA..........LL
MHR3-H9
TRPM1 571 DIGLVLEYLMGGAYRCNYTRKNFRTLYNNLFGPKRP.....KALKLLGMEDDE.....PPAKGKK
TRPM2 560 HVAQVLRELLGDFTQPLYPRPRHNDRLRLLL.PVPH.....VKLNVQG.....VSL....
TRPM3 594 DIGLVIEYLMGGAYRCNYTRKRFRTLYHNLFGPKRP.....KALKLLGMEDDI.....PLRRGR.
TRPM4 502 DVGHVLRMLLGKMCAPRYPSGGAWDPHPG.....QG.....F.G....
TRPM5 465 EVSRVLKDFLQDACRGFYQDGRPGDRRRAE.....
TRPM6 512 DIGLVVEYLIGRAYRSNYTRKHFRALYNNLYRKYKH.....QR.HSSGNRNESAESTLHSQFIRTAQPYKFKEKSIVL....
TRPM7 511 DIGLVIEYLMGGTYRCTYTRKRFRLIYNSLGGNNRRSGRNTSSSTPQLRKSHESFGNRADKKEKMRHNHFIKTAQPYRPKIDTVME....
TRPM8 522 T...FVWKLVANFRRGFRK.....
MHR4-H1
MHR4-H2
MHR4-H3
MHR4-H4
TRPM1 626 KKKKKKEEEIDIDVDDPAVSRFQYPFHELMVWAVLMKRQKMAVFLWQRGEESMAKALVACKLYKAMAHESSESDLVDDISQDLDNNSKDF
TRPM2 605 RSLYKRSSG.....HVTFTMDPIRDLLIWAIVQNRRELAGIIWAQSQDCIAAALACSKILKELSKEEEDTDSSEEM....LALAEEY
TRPM3 648 KTTKKREEEVDIDLDDPEINHFPFPFHELMVWAVLMKRQKMALFFWQHGEEAMAKALVACKLCKAMAHEASENDMVDDISQELNHNSRDF
TRPM4 535 ESMYLLSDKATSPLSL.DAGLGQAPWSDLLLWALLLNRAQMAMYFWEMGSNAVSSALGACLLLRVMARLEPDAEEAARR....KDLAFKF
TRPM5 495 KGPAKRPTGQKWLL.D.LNQKSENPWRDLFLWAVLQNRHEMATYFWAMGQEGVAAALAACKILKEMSHLETEAEAARAT....REA..KY
TRPM6 584 HKSRKKSKEQNVS.DDPESTGFLYPYNDLLVWAVLMKRQKMAMFFWQHGEEATVKAVIACILYRAMAHEAKESHMVDDASEELKNYSKQF
TRPM7 597 EGKKKRTKDEIVDIDDPETKRFPYPLNELLIWACLMKRQVMARFLWQHGEESMAKALVACKIYRSMAYEAKQSDLVDDTSEELKQYSNDF
TRPM8 538 .EDRNGRDEMDIELHD.VSPITRHPLQALFIWAILQNKKELSKVIWEQTRGCTLAALGASKLLKTLAKVKNDINAAGES....EELANEY
C
TRPM2
TRPM4
TRPM7
TRPM8
extracellular
intracellular
Gβγ
90°

Fig. S8. Sequence comparison of TRPM3 in different species and different TRPM orthologues, together with 3D models of the MHR3-4 linker (corresponding to the exon 17-encoded part of TRPM3) of different TRPM channel proteins. (*A*) Alignment of the primary protein sequence of TRPM3 proteins from a wide variety of vertebrate species. Shown is the region homologous to the region encoded by exons 16 and 17 and the N-terminal part of exon 18 of mouse TRPM3. Blue coloration indicates complete conservation of the sequence across the 14 species depicted. Colors progressing to yellow and reddish hues indicate progressively less conservation. In the lower graph, the consensus sequence is given, together with a graphical representation of how many of the individual sequences conform to the consensus sequence. Note the high overall degree of conservation which is especially high in the region encoded by exon 17. The NCBI accession numbers of the sequences are: *Homo sapiens* (human): XP_011517338; *Mus musculus* (mouse): NP_001030319; *Monodelphis domestica* (opossum): XP_016279167; *Ornithorhynchus anatinus* (platypus): XP_028911055; *Crocodylus porosus* (crocodile): XP_019410753; *Corvus cornix* (crow): XP_019137495; *Gallus gallus* (chicken): XP_025000670; *Xenopus tropicalis* (frog): XP_012827177; *Sander lucioperca* (zander): XP_031161818; *Danio rerio* (zebrafish): XP_021332142; *Callorhinchus milii* (elephant shark): XP_007904772; *Rhincodon typus* (whale shark): XP_020365728; *Petromyzon marinus* (lamprey): XP_032800301; *Latimeria chalumnae* (Latimeria, coelacanth): XP_014347481. Please note that some of these sequences are marked as "predicted" and might also be only partial (for example the sequence for Latimeria). (*B*) Sequence alignment of the MHR3-4 linker region of human TRPM proteins. Positions with identical amino acids are highlighted in red and with similar amino acids in yellow. A high proportion of similarity and homology is found in the α-helical regions of the MHRs (labeled according to ref. 27), but the linker region (containing exon 17-encoded amino acids, blue lettering) is strongly divergent. Gray background indicates amino acids shown in red in *C*, gaps in gray background are due to amino acids not included (built) in the 3D structures. (*C*) Cartoon representation of 4 TRPM channels, for which 3D structures are available (PDB designations for TRPM2: 6MIX, ref. 28; TRPM4: 6BWI, ref. 29; TRPM7: 6BWF, ref. 30; TRPM8: 6NR3, ref. 31). The four subunits of each channel are shown in different blueish hues. The part located between MHR3 and MHR4 (often only partially built) is represented in red. Top row shows a view parallel to the membrane surface, the view of the bottom row is from the extracellular space perpendicular to the membrane. Additionally, the structure of Gβγ in complex with the TRPM3 exon 17-encoded peptide as reported in this paper is shown next to the structure of TRPM7 (blue: $G\beta_1$, cyan: $G\gamma_2$, orange: TRPM3 peptide). The cartoon of Gβγ was oriented and placed relative to the plasma membrane as reported by ref. 32 for GIRK2 channels in complex with Gβγ. The MHR3-4 linker is located on a similar position of the cytosolic surface on all four TRPM structures, indicating that the location of the MHR3-4 linker in TRPM3 channels (for which a full-length structure is not yet available) might be in a similar position. This position is easily within reach for Gβγ proteins tethered to the membrane.

A

SIGK Peptide: SIGKAFKILGYPDYD

TRPM3 Exon 17 Peptide: K_{592}RPKALKLLGMEDDI$_{606}$

** ***

B

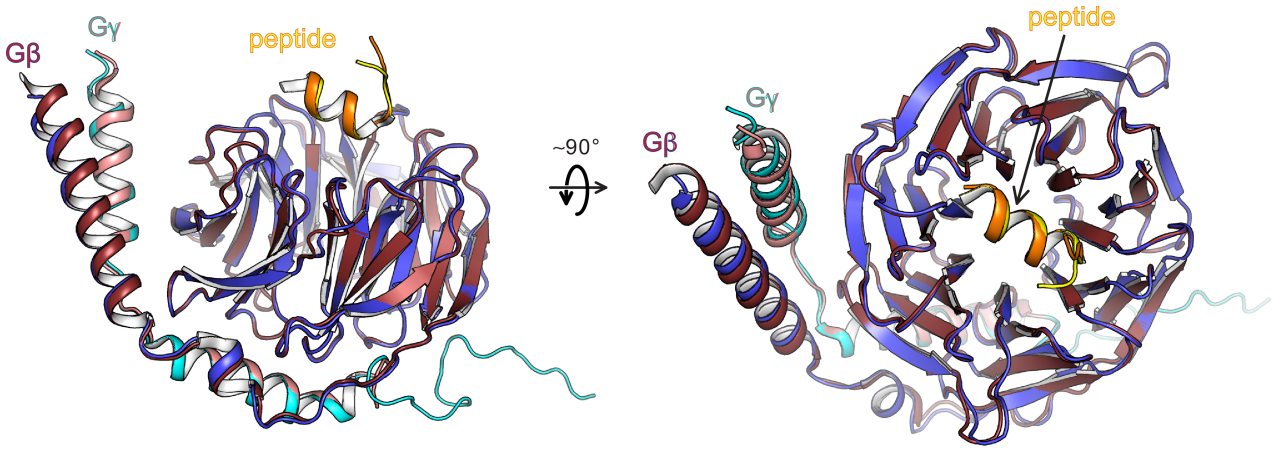

Fig. S9. The SIGK peptide (PDB: 1XHM, ref. 21) adopts a similar binding pose on Gβγ as the TRPM3 exon 17-encoded peptide. (*A*) Sequence alignment of the SIGK and the TRPM3 exon17-encoded peptide. The amino acids showing sequence homology or high similarity are printed in red. Asterisks indicate the amino acids identified in this manuscript as functionally highly important for the interaction of TRPM3 with Gβγ. Note that the TRPM3 peptide encompasses N-terminally two amino acids belonging to exon 16 (KR) and C-terminally three amino acids belonging to exon 18 (DDI). (*B*) Overlay of the cocrystal structures of SIGK and the exon17-encoded peptides, each bound to Gβγ. The cocrystal structure reported in this manuscript is colored as in Fig. 3*A* (Gβ in blue, Gγ in cyan, TRPM3 peptide in orange). The Gβγ cocrystallized with the SIGK peptide is shown in dark red (Gβ) and light red (Gγ) while the SIGK peptide itself is depicted in yellow. Both structures are highly similar (RMSD of 0.42 Å) and the peptides show the same orientation and overall binding conformation.

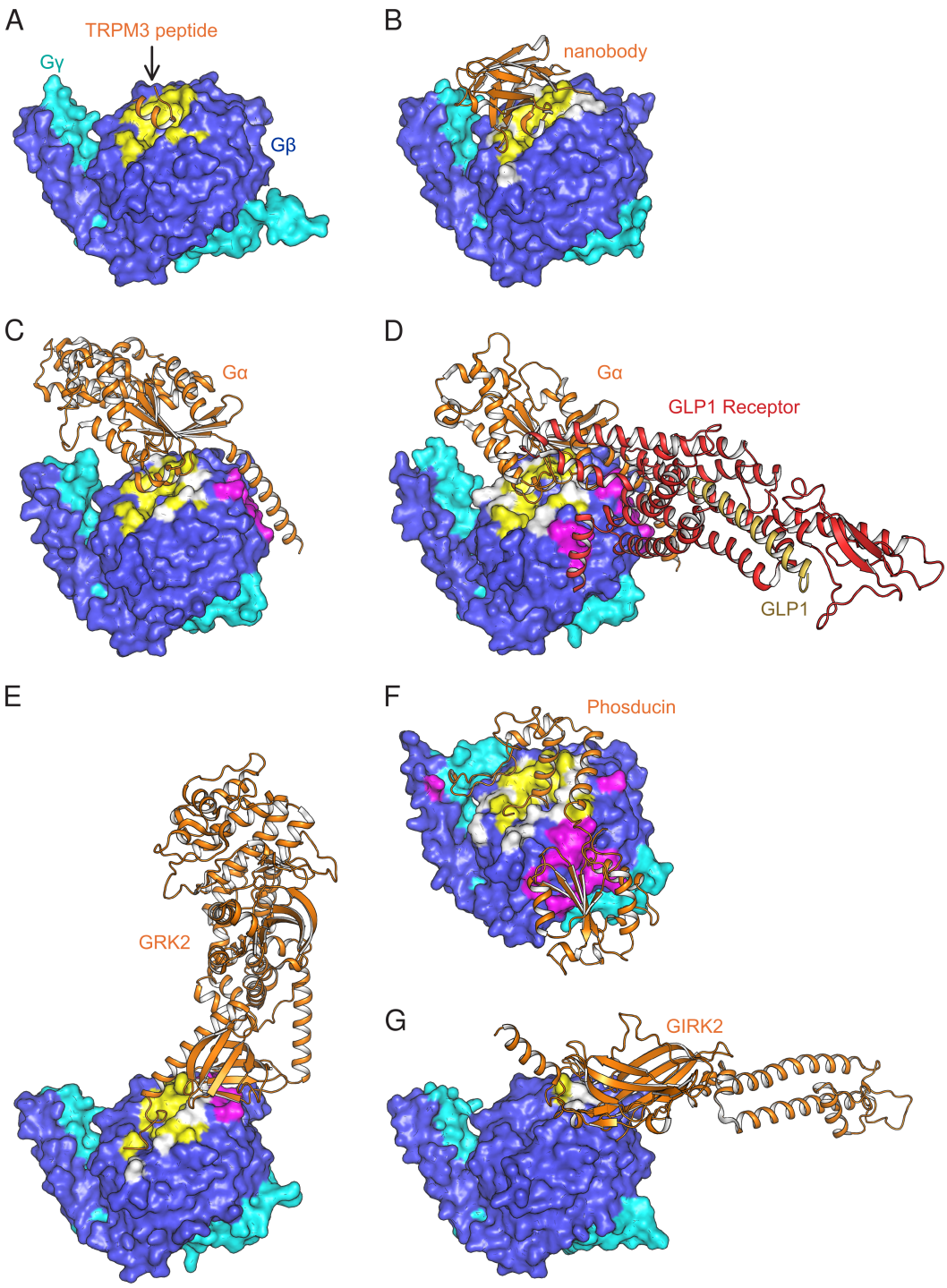

Fig. S10. Comparison of docking sites of different binding partners of Gβγ. Structures of Gβγ in complex with interaction partners are shown in the same orientation. The main Gβγ interaction partner is depicted in cartoon representation in orange, further interaction partners (if available) in red and yellow. Gβγ is depicted in surface representation, with Gγ colored in cyan and Gβ principally in blue. (*A*) Gβ residues that interact with TRPM3 exon 17 peptide are colored in yellow, also in all other structures (*B* – *G*), in which these residues undergo interactions. Additional residues at this interface are colored white if they are involved in inter-

actions with another binding partner. Gβγ residues that undergo interactions at other interfaces are colored magenta. The shown interaction partners are (*A*) TRPM3 exon17 peptide (this work), (*B*) a Gβγ-binding nanobody (PDB: 6B20, ref. 33), (*C*) Gα (PDB: 5KDO, ref. 34), (*D*) Gα (orange) bound to glucagon-like peptide-1 (GLP1) receptor (red), which has also GLP1 (yellow) bound (PDB: 5VAI, ref. 35), (*E*) G protein-coupled receptor kinase 2 (PDB: 5UKL, ref. 36), (*F*) phosducin (PDB: 2TRC, ref. 37), and (*G*) the ion channel GIRK2 (PDB: 4KFM, ref. 32).

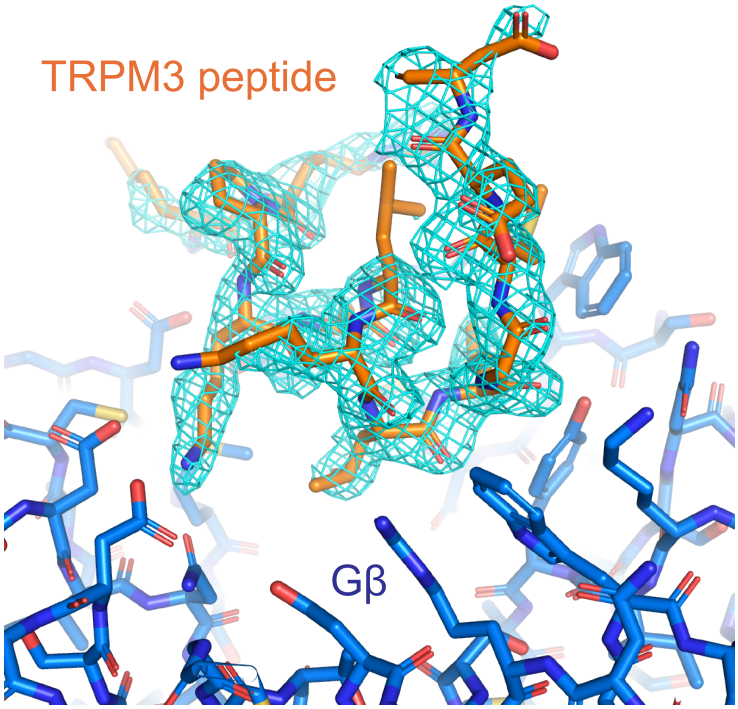

Fig. S11. Omit map. A composite omit map using simulated annealing was created with Phenix and is shown at a contour level of 1 σ (cyan mesh) in a radius of 1.5 Å around atoms belonging to the TRPM3 peptide (orange). The peptide and Gβ (blue) are shown in stick representation.

Table S1. Crystallographic data collection and refinement statistics.

Crystallographic statistics	
Wavelength (Å)	0.9754
Space group	$P2_12_12_1$
a, b, c (Å)	45.86, 80.43, 113.59
α, β, γ (°)	90, 90, 90
Resolution limits (Å)	42.52 – 1.94 (2.01 – 1.94)
Rmerge (%)	7.3 (128)
Rmeas (%)	8.7 (151)
Rpim (%)	4.6 (79.5)
〈I/σ〉	13.2 (1.4)
CC1/2 (%)	99.9 (52.8)
Multiplicity	6.5 (6.7)
Completeness (%)	99.3 (98.3)
Total number of reflections	205,787 (20,381)
Number of unique reflections	31,659 (3,044)
Refinement and model statistics	
Rwork (%)	18.8
Rfree (%)	22.4
Bond length root mean square deviation (Å)	0.007
Bond angle root mean square deviation (°)	1.21
Ramachandran plot favored/outliers (%)	96 / 0.2

Statistics for the highest-resolution shell are shown in parentheses.

Supplementary References

1. J. A. Iñiguez-Lluhi, M. I. Simon, J. D. Robishaw, A. G. Gilman, G protein βγ subunits synthesized in Sf9 cells. Functional characterization and the significance of prenylation of γ. *J. Biol. Chem.* **267**, 23409-23417 (1992).
2. T. Kozasa, Purification of G protein subunits from Sf9 insect cells using hexahistidine-tagged α and βγ subunits. *Methods Mol. Biol.* **237**, 21-38 (2004).
3. J. Przibilla *et al.*, Ca^{2+}-dependent regulation and binding of calmodulin to multiple sites of Transient Receptor Potential Melastatin 3 (TRPM3) ion channels. *Cell Calcium* **73**, 40-52 (2018).
4. S. Dembla *et al.*, Anti-nociceptive action of peripheral mu-opioid receptors by G-beta-gamma protein-mediated inhibition of TRPM3 channels. *eLife* **6**, e26280 (2017).
5. J. Frühwald *et al.*, Alternative splicing of a protein domain indispensable for function of transient receptor potential melastatin 3 (TRPM3) ion channels. *J. Biol. Chem.* **287**, 36663-36672 (2012).
6. J. Oberwinkler, A. Lis, K. M. Giehl, V. Flockerzi, S. E. Philipp, Alternative splicing switches the divalent cation selectivity of TRPM3 channels. *J. Biol. Chem.* **280**, 22540-22548 (2005).
7. M. Bünemann, M. Frank, M. J. Lohse, Gi protein activation in intact cells involves subunit rearrangement rather than dissociation. *Proc. Natl. Acad. Sci. U.S.A.* **100**, 16077-16082 (2003).
8. M. Behrendt, J. Polaina, H. Y. Naim, Structural hierarchy of regulatory elements in the folding and transport of an intestinal multidomain protein. *J. Biol. Chem.* **285**, 4143-4152 (2010).
9. T. F. J. Wagner *et al.*, TRPM3 channels provide a regulated influx pathway for zinc in pancreatic beta cells. *Pflügers Archiv* **460**, 755-765 (2010).
10. A. Drews *et al.*, Structural requirements of steroidal agonists of transient receptor potential melastatin 3 (TRPM3) cation channels. *Br. J. Pharmacol.* **171**, 1019-1032 (2014).
11. A. D. Edelstein *et al.*, Advanced methods of microscope control using μManager software. *Journal of Biological Methods* **1**, e10 (2014).
12. D. Badheka *et al.*, Inhibition of Transient Receptor Potential Melastatin 3 ion channels by G-protein βγ subunits. *eLife* **6**, e26147 (2017).
13. C. Grimm, R. Kraft, S. Sauerbruch, G. Schultz, C. Harteneck, Molecular and functional characterization of the melastatin-related cation channel TRPM3. *J. Biol. Chem.* **278**, 21493-21501 (2003).
14. M. G. Leitner *et al.*, Direct modulation of TRPM4 and TRPM3 channels by the phospholipase C inhibitor U73122. *Br. J. Pharmacol.* **173**, 2555-2569 (2016).
15. C. Hu, S. D. Depuy, J. Yao, W. E. McIntire, P. Q. Barrett, Protein kinase A activity controls the regulation of T-type CaV3.2 channels by Gβγ dimers. *J. Biol. Chem.* **284**, 7465-7473 (2009).
16. M. D. Abràmoff, P. J. Magalhães, S. J. Ram, Image processing with ImageJ. *Biophotonics Int.* **11**, 36-42 (2004).
17. C. A. Schneider, W. S. Rasband, K. W. Eliceiri, NIH Image to ImageJ: 25 years of image analysis. *Nat. Methods* **9**, 671-675 (2012).
18. W. Kabsch, XDS. *Acta Crystallogr. D Biol. Crystallogr.* **66**, 125-132 (2010).
19. M. D. Winn *et al.*, Overview of the CCP4 suite and current developments. *Acta Crystallogr. D Biol. Crystallogr.* **67**, 235-242 (2011).
20. A. J. McCoy *et al.*, Phaser crystallographic software. *J. Appl. Crystallogr.* **40**, 658-674 (2007).

21. T. L. Davis, T. M. Bonacci, S. R. Sprang, A. V. Smrcka, Structural and molecular characterization of a preferred protein interaction surface on G protein βγ subunits. *Biochemistry* **44**, 10593-10604 (2005).
22. P. Emsley, B. Lohkamp, W. G. Scott, K. Cowtan, Features and development of Coot. *Acta Crystallogr. D Biol. Crystallogr.* **66**, 486-501 (2010).
23. G. N. Murshudov, A. A. Vagin, A. Lebedev, K. S. Wilson, E. J. Dodson, Efficient anisotropic refinement of macromolecular structures using FFT. *Acta Crystallogr. D Biol. Crystallogr.* **55**, 247-255 (1999).
24. R. P. Joosten, K. Joosten, G. N. Murshudov, A. Perrakis, PDB_REDO: constructive validation, more than just looking for errors. *Acta Crystallogr. D Biol. Crystallogr.* **68**, 484-496 (2012).
25. P. D. Adams *et al.*, PHENIX: a comprehensive Python-based system for macromolecular structure solution. *Acta Crystallogr. D Biol. Crystallogr.* **66**, 213-221 (2010).
26. L. Mavridis, R. W. Janes, PDB2CD: a web-based application for the generation of circular dichroism spectra from protein atomic coordinates. *Bioinformatics (Oxford, England)* **33**, 56-63 (2017).
27. H. E. Autzen *et al.*, Structure of the human TRPM4 ion channel in a lipid nanodisc. *Science* **359**, 228-232 (2018).
28. L. Wang *et al.*, Structures and gating mechanism of human TRPM2. *Science* **362**, eaav4809 (2018).
29. J. Duan *et al.*, Structure of full-length human TRPM4. *Proc. Natl. Acad. Sci. U.S.A.* **115**, 2377-2382 (2018).
30. J. Duan *et al.*, Structure of the mammalian TRPM7, a magnesium channel required during embryonic development. *Proc. Natl. Acad. Sci. U.S.A.* **115**, E8201-E8210 (2018).
31. Y. Yin *et al.*, Structure of the cold- and menthol-sensing ion channel TRPM8. *Science* **359**, 237-241 (2018).
32. M. R. Whorton, R. MacKinnon, X-ray structure of the mammalian GIRK2-βγ G-protein complex. *Nature* **498**, 190-197 (2013).
33. S. Gulati *et al.*, Targeting G protein-coupled receptor signaling at the G protein level with a selective nanobody inhibitor. *Nat. Commun.* **9**, 1996 (2018).
34. A. I. Kaya *et al.*, A conserved hydrophobic core in $G\alpha_{i1}$ regulates G protein activation and release from activated receptor. *J. Biol. Chem.* **291**, 19674-19686 (2016).
35. Y. Zhang *et al.*, Cryo-EM structure of the activated GLP-1 receptor in complex with a G protein. *Nature* **546**, 248-253 (2017).
36. H. V. Waldschmidt *et al.*, Structure-based design of highly selective and potent G protein-coupled receptor kinase 2 inhibitors based on paroxetine. *J. Med. Chem.* **60**, 3052-3069 (2017).
37. R. Gaudet, A. Bohm, P. B. Sigler, Crystal structure at 2.4 Å resolution of the complex of transducin βγ and its regulator, phosducin. *Cell* **87**, 577-588 (1996).